EVALUATION AND ANALYSIS OF SEASAT-A SCANNING MULTICHANNEL MICROWAVE RADIOMETER (SMMR) ANTENNA PATTERN CORRECTION (APC) ALGORITHM

FINAL REPORT FOR SUB-TASK 1: 6.6 GHz T_B VS. $T_{surface\ truth}$ COMPARISON RESULTS

Prepared under JPL contract number 955368 by:

S. N. Kitzis
J. L. Kitzis

Environmental Sensing Algorithm Development Company

8238 Fenwick Street
Sunland, California 91040

March 16, 1979

(NASA-CR-158367) EVALUATION AND ANALYSIS OF SEASAT A SCANNING MULTICHANNEL MICROWAVE RADIOMETER (SMMR) ANTENNA PATTERN CORRECTION (APC) ALGORITHM Final Report (Environmental Sensing Algorithm Development) 84 p HC G3/32

N79-20298

Unclas 16675

This work was performed for the Jet Propulsion Laboratory, California Institute of Technology sponsored by the National Aeronautics and Space Administration under Contract NAS7-100.

This report contains information prepared by Environmental Sensing Algorithm Development Company under JPL sub-contract. Its content is not necessarily endorsed by the Jet Propulsion Laboratory, California Institute of Technology, or the National Aeronautics and Space Administration.

ABSTRACT

This report documents the first part of a three-part study whose overall objective is an initial assessment of the accuracy of the SEASAT-A SMMR Antenna Pattern Correction (APC) algorithm. Interim APC brightness temperature measurements for the SMMR 6.6 GHz channels are compared with surface truth derived sea surface temperatures. Plots and associated statistics are presented for SEASAT-A SMMR data acquired for the Gulf of Alaska experiment (GOASEX). The most important conclusion of the study concerns apparent cross-track gradients observed in the 6.6 GHz brightness temperature data.

CONTENTS

CONTENTS (Continued)

FIGURE

CONTENTS (Continued)

CONTENTS (Continued)

TABLE

1.0 SUMMARY

This report documents the first part of a three-part study whose overall objective is an initial assessment of the accuracy of the SMMR Antenna Pattern Correction Algorithm. Interim APC brightness temperature measurements for the SMMR 6.6 GHz vertical and horizontal polarization channels are compared to surface truth derived sea surface temperatures. Plots of brightness temperature versus sea surface temperature and associated statistics are presented for various combinations of the SEASAT-A passes acquired for the Gulf of Alaska experiment (GOASEX). For the purpose of establishing a reference curve, the study makes use of a model developed for an integrated water vapor content of 2.4 grams/cm^2, a wind speed between zero and seven meters/sec, and cloud-free conditions.

The most important conclusions of the study are:

(1) There appear to exist opposing cross-track gradients in the vertical and horizontal 6.6 GHz brightness temperatures output by the interim APC algorithm.

(2) For both vertical and horizontal brightness temperature data, the observed bias with respect to the model-predicted reference curve is least for cell 4 data, and progressively increases in magnitude from cell 4 to cell 1.

(3) If the observed biases are removed from the measured brightness temperature data, the resulting values agree quite well with model-predicted values (1.5°K for V and 2.6°K for H).

2.0 INTRODUCTION

2.1 Problem Statement. The SEASAT-A Scanning Multichannel Microwave Radiometer (SMMR) is designed to make measurements of thermal microwave emission from the Earth for the primary purpose of determining sea surface temperatures, wind speed, and atmospheric water vapor and liquid water parameters. The antenna temperatures measured by the SMMR contain known antenna pattern effects which must be removed before these measurements can be used to derive geophysical parameters. The Antenna Pattern Correction (APC) Algorithm has been designed by E. G. Njoku and coded by R. E. Cofield to remove these effects. In brief summary, the APC algorithm accepts as input SMMR antenna temperature (T_A) measurements and produces corrected brightness temperatures (T_B) as its output. These output brightness temperatures are then used as inputs to the geophysical parameter algorithms. The problem to be addressed here is the evaluation of the accuracy of the APC brightness temperature outputs.

This report documents the first part of a three-part study whose overall objective is an initial assessment of the accuracy of the APC algorithm. As the SMMR algorithms mature, and as a larger data set becomes available, it is expected that further studies will refine the results presented here. The three parts of this initial assessment are:

A. <u>6.6 GHz T_B vs. $T_{surface\ truth}$ Comparison</u>

T_B measurements for the SMMR 6.6 GHz channels are compared to surface truth derived sea surface temperatures. The two 6.6 GHz channels are used because they are most sensitive to sea surface temperature (SST) but least sensitive to atmospheric effects. SST measurements are more numerous and more accurate than other types of surface truth measurements. Thus, the comparison of 6.6 GHz T_B with SST under clear atmospheric conditions provides a large, high-quality data set from which to assess the accuracy of the APC algorithm.

B. <u>T_B Measured vs. T_B Calculated Comparison</u>

T_B measurements for all ten SMMR channels are compared with T_B values calculated from geophysical models using surface truth data. Although this task is restricted to a smaller surface truth data set than task A, it assesses the accuracy of all ten SMMR channels rather than only two of them. In addition, this task is less dependent on using clear atmospheric conditions since the models take atmospheric variations into account.

C. <u>T_A vs. T_B Comparison</u>

T_A measurements for all ten SMMR channels are compared with the corresponding T_B outputs. This comparison allows a determination of whether the APC algorithm adequately removes those instrument effects known to be present in the T_A data.

The results obtained for task A are the subject of this document.

2.2 <u>Brief Description of the APC Algorithm</u>. At this time, the APC algorithm has not yet reached its final form. Section 2.2.1 describes the full set of capabilities to be implemented in the final APC algorithm. Section 2.2.2 outlines the subset presently implemented in the interim version of the APC. The results of this study are based only on output obtained from the interim APC. It is expected that a later study will perform a similar evaluation of the final APC.

2.2.1 <u>Final APC Description</u>. The input T_A data to the APC algorithm consists of measurements of microwave emission at ten different channels. Each channel is characterized by one of five frequencies (6.6, 10.69, 18, 21, and 37 GHz) and one of two polarizations (vertical and horizontal).

The T_A measurements are sampled at regular time intervals along the SMMR scan, which results however in an irregular spacing of points on the Earth's surface. The APC algorithm outputs T_B data in the form of square arrays of data cells which are uniformly distributed within the SMMR swath. There are four different array sizes which are referred to as Grids 1, 2, 3, and 4. The ten channels are output on the four grids as shown in Table 1.

The final APC algorithm performs the following operations:

(a) Read SMMR T_A data.

(b) Average T_A data into grid cells.

(c) Correct T_A cells for Faraday rotation.

(d) Correct T_A cells for non-nominal incidence angles.

(e) Correct T_A cells for cross-polarization an enna pattern effects.

(f) Correct T_A cells for polarization rotation effects due to scan motion.

(g) Correct T_A cells for sidelobe contributions from within the SMMR swath, from outside the SMMR swath but on the Earth's surface, and from space.

(h) Output SMMR T_B data and associated quality flags.

2.2.2 Interim APC Description. The interim version of the APC algorithm performs the following subset of the final APC operations:

(a) Read SMMR T_A data.

(b) Average T_A data into grid cells.

(c) Correct T_A cells for cross-polarization antenna pattern effects.

(d) Correct T_A cells for polarization rotation effects due to scan motion.

(e) Correct T_A cells for sidelobe contributions from space.

(f) Output SMMR T_B data.

Note that the interim APC does not include corrections for Faraday rotation, incidence angles, or Earth sidelobe contributions, nor does it calculate data quality flags.

2.3 General Evaluation Approach. Although this study makes maximum use of available resources, any attempt to evaluate the APC at this time is subject to the following constraints:

(a) The final version of the APC is still under development, and so only the interim version may be used.

(b) The only large body of SMMR data which has been processed thus far through the SMMR interim APC consists of fifteen passes through the northeast Pacific Ocean obtained during the Gulf of Alaska SEASAT Experiment (GOASEX) in Sept. 1978.

(c) Turnaround time for obtaining additional data is on the order of several weeks.

In line with the above constraints, the general approach followed in this study is outlined below:

(1) Although the final APC is not complete, make use of the 6.6 GHz grid 1 data from the interim APC.

(2) Make maximum use of the immediately available GOASEX data although it is not the best data set for this type of evaluation.

(3) Request additional data, to be used if time permits.

(4) Digitize the National Marine Fisheries Service (NMFS) map of average Sea Surface Temperatures (SST) for the month of September 1978 so that it can be used as a source of surface truth measurements.

(5) Make use of JPL subroutine libraries to produce computer-generated plots of SMMR T_B versus SST and to produce associated statistical information.

(6) Generate separate plots and statistics for each column of the 6.6 GHz T_B grids in order to identify any effects which may vary across the SMMR swath.

(7) Use a radiative transfer model relating SMMR T_B to SST as a reference curve against which to compare the actual data points.

(8) Perform supplementary studies if a need arises and time permits.

The above approach is designed to provide an adequate and flexible framework from which to assess the accuracy of the APC algorithm in producing 6.6 GHz T_B data values.

3.0 TECHNICAL DISCUSSION

3.1 Reference Model. Radiative transfer and the physics of the ocean surface and atmosphere allow T_B to be modeled as a function of sea surface temperature, wind speed, and integrated atmospheric water vapor content, assuming that cloud-free conditions prevail. The primary variable of these models is sea surface temperature. Wind speed and water vapor content serve to shift the basic model curve towards higher or lower T_B values but do no appreciably affect its overall shape.

For a standard atmosphere and several different values of integrated water vapor content, R. Hofer has produced from basic geophysical models (which assume cloud-free conditions) a set of polynomial coefficients which express T_B as a second-order function of sea surface temperature with an additional linear dependence on wind speed. Each of these functions is of the form

$$T_B = a_0 + a_1 T_s + a_2 T_s^2 + bv$$

where

T_s = sea surface temperature (^oK)

v = max [wind speed (meters/sec), 7]

The value of v used in the above equation is either the actual wind speed or a constant 7 meters/second since the observed T_B is independent of this parameter for wind speeds below 7 meters/second.

For the purpose of establishing a reference against which to compare the plotted 6.6 GHz T_B - SST pairs, this study uses the model polynomials developed for an integrated water vapor content of 2.4 grams/cm^2, a wind speed between zero and seven m/sec, and cloud-free conditions. These polynomials are given in Figure 1.

The 2.4 grams/cm^2 figure is close to the global average value for integrated water vapor content. The exact value chosen is not critical since variations in integrated water vapor content do not appreciably alter the shape of the reference curve but merely shift it up or down by about half a degree Kelvin per gram/cm^2.

The wind speed range of 0 to 7 m/s is commonly observed over the ocean surface and should serve as a lower limit to the observed T_B - SST pairs. Wind speeds higher than 7 m/sec will not alter the shape of the reference curve but will shift it upwards by about half a degree Kelvin per m/s for the 6.6 GHz vertical polarization and by about twice this amount for the horizontal polarization.

Thus, the majority of the plotted T_B - SST pairs should lie near the chosen reference curves, except when wind speeds exceed 7 m/sec or when fairly dense clouds are present.

3.2 Data Selection. The major difficulty which plagues an evaluation of this type is that of acquiring spacecraft and surface truth data sets which are matched in location and time. The additional requirement for low wind speed, clear atmosphere conditions further compounds the problem. Since Geostationary Orbiting Environmental Satellite (GOES) visible and infrared images were available for the month of September, 1978, a search was made for clear atmospheric conditions during this month. As a result, over fifty time spans were identified during which the SEASAT-A SMMR viewed the open ocean with little or no intervening cloud cover. Unfortunately, spacecraft data for these times other than that already obtained for the GOASEX workshop was not available and could not be obtained in time to be included in this Task A effort.

3.2.1 Spacecraft Data Set. The GOASEX data set consists of fifteen passes through the northeastern Pacific Ocean during September, 1978. One pass contains numerous data gaps and is completely useless for evaluation purposes. Two other passes of the fifteen are also useless since the SMMR field of view is completely over land. Of the remaining twelve passes, two are ascending (south to north) and ten are descending. The two ascending passes parallel the U.S. and Canadian west coasts so closely that the SMMR data is corrupted by sidelobe effects from the adjacent land. In addition, many of the GOASEX passes were chosen for "interesting" weather patterns, which is the opposite of the clear weather conditions needed for this study. In light of these problems, the GOASEX passes are not an ideal data set for a SMMR APC evaluation effort. However, they do have the advantage of being readily available and so are used in this study.

3.2.2 Sea Surface Temperature Data Set. Sea surface temperature data is available in two major forms: 1) individual spot reports made by ship or buoy and 2) smoothed continuous temperature fields produced from these spot reports. This study uses sea surface temperature field data rather than spot reports in order to simplify the process of matching spacecraft data with SST data. SST fields are available for both the north Pacific and the north Atlantic, but since the available spacecraft data is currently restricted to the GOASEX passes, only one SST field covering the northeastern Pacific for September, 1978 is needed for this study.

The NMFS September 1978 mean SST field for the northeastern Pacific has been digitized to a one degree latitude/longitude resolution and put into machine-readable form as part of this study. Figure 2.1 shows the original NMFS contour map. The dark outline contains that portion which has been digitized. Figure 2.2 shows a contour map produced from the digitized values and confirms the success of the digitization effort. The NMFS monthly average accuracy is known to be about 1 to 2 degrees Celsius. The digitization accuracy is estimated at 0.2°C, which is insignificant when compared with the original error.

3.3 Software Development. Various pieces of software have been developed in the course of this study. This section presents a brief description of the development process and the outputs produced by each program. The software development process has been characterized by the maintenance of a small test case which can be repeated each time changes are made to existing software. In this manner, the implementation of each change may be checked with minimum effort. All numerical results have been checked with the aid of a programmable hand calculator. Maximum use has been made of JPL subroutine libraries in obtaining plotting and statistics software. Development time has been kept to a minimum by following the above strategy.

3.3.1 Reading IGDR Files. The output T_B data from the APC algorithm are written onto what is called a SMMR IGDR basic sensor file. The data on this file is in a packed format compatible with the JPL IBM 360/75 machine and must be converted into a format compatible with the JPL UNIVAC 1108 computer used for this study. This conversion was accomplished using a set of subroutines developed by W. D. McFaddin and modified by J. Kitzis. The reformatted data for all grids has been written to tape for use in later tasks. This procedure is more efficient than reformatting the data each time it is used.

3.3.2 T_B Vs. SST Plots and Statistics. The primary software analysis tool developed for this study produces plots of 6.6 GHz vertical and horizontal brighcness temperatures versus sea surface temperature, and associated statistics. The sea surface temperature values are linearly interpolated from the four closest points of the digitized SST field using the latitude and longitude associated with the T_B measurement. Four plots and printed statistics are produced each time the program is executed. The first two plots are produced for the 6.6 GHz vertical T_B data, while the last two plots are for horizontal data. Examples of all these outputs may be found in Table 3 and Figures 3.1 – 3.4.

In the first and third plots produced, as shown in Figures 3.1 and 3.3, each T_B – SST pair is plotted as a single Arabic numeral (1, 2, 3, or 4). The numeral indicates which column of the grid 1 array contains the T_B value. Column 1 measurements are nearest the spacecraft track, while Column 4 measurements are farthest. Each of these plots also contains two curves. The unmarked curve represents the polynomial (second order maximum) which fits all the data points best in a least squares sense. The curve marked with plus signs represents the standard atmosphere/low-wind-speed model curve for the appropriate polarization.

In the second and fourth plots (Figures 3.2 and 3.4), the model curves and the least-squares fitted curves are plotted as before. The fitted curves are now marked with the character "A". The previously plotted individual data points are replaced with a set of four curves, each curve representing the best fit in a least squares sense to one column of the grid 1 data points. The curve for each column is marked with the appropriate Arabic numeral (1, 2, 3, or 4).

The printed statistical output (Table 3) is divided into two sections. The upper section contains the three polynomial coefficients and the root-mean-square (RMS) statistic for the ten least squares fitted curves (all-data fits plus four column fits for both polarizations). The RMS statistic is calculated according to:

$$\mathrm{RMS} = \sqrt{\frac{\sum_{i=1}^{N} \left(T_{B_i} - p(SST_i)\right)^2}{N}} \qquad \text{Eq. 1}$$

where

T_{B_i} = i^{th} T_B value

SST_i = associated SST value

$p(SST_i)$ = fitted polynomial evaluated for the i^{th} SST value

N = total number of data points

The lower section of the printout contains a bias and an RMS statistic around a biased model curve for the ten data groups represented by all the vertically polarized data (V), all the horizontally polarized data

(H), and the four individual columns of data for each polarization. The bias is calculated according to:

$$\text{Bias} = \frac{\sum_{i=1}^{N} \left(T_{B_i} - m\,(SST_i) \right)}{N} \qquad \text{Eq. 2}$$

where

$m(SST_i)$ = model polynomial evaluated for the ith SST value

and

T_{B_i}, SST_i, and N are as defined above.

The corresponding RMS statistic is calculated according to:

$$\text{RMS} = \sqrt{\frac{\sum_{i=1}^{N} \left(T_{B_i} - \text{Bias} - m(SST_i) \right)^2}{N}} \qquad \text{Eq. 3}$$

where

T_{B_i}, $m(SST_i)$, SST_i, and N are as defined above, and the bias is as defined above for the appropriate data group.

3.3.3 Cross-Track Gradient Vs. Latitude. A secondary software analysis tool developed as a supplement to the primary study produces a plot (Figure 11.1) of the 6.6 GHz T_B gradient across the SMMR swath versus latitude, and associated statistics (Table 11.1). A first-order polynomial is fitted in a least squares sense to each row of T_B values in the 6.6 GHz grid 1 array. The slope of this line for each row is plotted against the average latitude for the row. The character "V" is plotted for V data, and the character "H" for H data.

The printed statistical output includes the average latitude, the two polynomial coefficients, and the RMS statistic for each row of T_B data for both polarizations. The RMS is calculated as shown previously in Equation 1 except that the polynomial is now a function of cell number rather than SST.

3.3.4 T_B Minus Model T_B Vs. Incidence Angle. Another secondary software analysis tool developed as a supplement to the primary study produces a plot (Figure 11.2) of the difference between the measured 6.6 GHz T_B and the model-predicted T_B (ΔT_B) versus incidence angle, and associated statistics (Table 11.2). The model-predicted T_B is calculated according to the equations given in Figure 1, which assume an integrated water vapor content of 2.4 g/cm^2 and a wind speed between zero and seven meters/sec. The SST values for the equations are obtained by linearly interpolating the digitized SST field. Each ΔT_B — incidence angle pair is plotted as a single character: "V" for V data and "H" for H data.

A second order polynomial is fitted in the least squares sense to ΔT_B as a function of incidence angle. Separate fits are made for the V data and the H data. The printed statistical output includes the three polynomial coefficients and the RMS statistic for both least squares fits. The RMS statistic is calculated as shown previously in Equation 1 except that the polynomial is now a function of incidence angle rather than SST, and ΔT_{B_i} replaces T_{B_i}.

3.4 Discussion of Results. Most of the tangible results of this study are in the form of computer plots and printouts generated by the software described in the previous section. A summary of the runs made for the study may be found in Table 2. RUN1 and RUN2 were test cases used only to check out the software and will not be discussed further. Runs 3 through 10 are executions of the T_B vs. SST software package and constitute the principal analysis performed for this study. These are designated as Type A runs in Table 2. The output of RUN3 consists of four plots and one table of statistics, which are respectively shown as Figures 3.1, 3.2, 3.3, 3.4, and Table 3. Similarly, Figures and Tables 4 through 10 display the outputs of Runs 4 through 10.

In addition to the primary analysis, three supplementary analyses were performed, two of which involved computer programs described in the previous section, while the third consisted of a brief survey of antenna temperature data which did not involve any programming efforts. Figure 11.1 and Table 11.1 contain the outputs of the cross-track gradient versus latitude program for the RUN 11 data blocks. These outputs are designated as Type B in Table 2. Similarly, Figure 11.2 and Table 11.2 contain the outputs of the ΔT_B versus incidence angle program for the same RUN 11 blocks. These outputs are designated as Type C in Table 2. In a similar manner, Figures and Tables 12 through 14 display the outputs of Runs 12 through 14.

All of the runs listed in Table 2 and the results of the antenna temperature data survey are discussed below.

3.4.1 Discussion of RUN 10. RUN 10 combines data from all of the descending GOASEX passes. The following observations are made regarding Table 10 and Figures 10.1 through 10.4:

(a) The fitted curves are roughly parallel to the model curves within the SST range for which data points are available. However, the fitted curves show less variation of T_B with sea surface temperature (smaller slope) than do the model curves. We suspect that sea surface roughness due to high wind speeds in the northern latitudes is causing the T_B values to be artificially high there and is obscuring the normal T_B dependence on SST. Wind speeds of up to 20 m/sec (~40 knots) have been observed in the northern portions of the GOASEX region. Wind speeds of this magnitude will raise the 6.6 GHz V data by about 7 degrees Kelvin and the 6.6 GHz H data by about 13 degrees Kelvin. The upward scatter of the actual data points agrees with these numbers.

(b) All the data shows more scatter in the direction of increasing T_B than in the downward direction. This effect is attributable to rain, dense water vapor clouds, and sea roughness due to high winds. The H data exhibits more scatter than does the V data, probably due to its greater sensitivity to ocean surface roughness.

(c) The V data points tend to fall below the model curve while the H data points usually lie above the model curve. Furthermore, the data from column 4 exhibits the best agreement with the model curves, and the data shows less agreement with the model as one moves from column 4 to column 1 data.

(d) The trends discussed in item (c) are confirmed by the bias statistics of Table 10. All biases around the model curves are negative for V data and positive for H data. In addition, the magnitudes of these biases increase from column 4 to column 1. This is strongly indicative of the existence of a cross-track bias in both the V and H T_B data. The direction of the bias in the V data is opposite that of the bias in the H data. Also, the change in the bias from column 4 to column 1 is almost twice as large for H data as for V data. However, many of the V and H data points have been raised in value by the effects of high winds, clouds, and rain. Hence, all of the data has been biased high by an unknown amount, and these unknown environmental biases for V and H should be subtracted from the biases in Table 10 to arrive at the true instrument biases. Therefore, it may very well be true that the instrument biases for both V and H are negative, with V more strongly biased than H. Further study is required to calculate the actual instrument biases.

(e) The RMS dispersion of all the V data about the biased model curve is about 1.5°K while that of the H data is about 2.6°K. These RMS dispersions exceed those about the best fitted V and

H curves by only about 10%. Hence, the biased model curves fit the data almost as well as the best fitted curves in the least squares sense. This is quite encouraging in view of the many known environmental effects, the suspected cross-track biases, and other possible instrument effects in the data. The fact that the RMS values for the H data exceed those for the V data by about 1°K is probably due to the greater sensitivity of the H data to high winds.

(f) The RMS values about the best fitted curves for columns 2 and 3 are smaller by about 0.2°K than those for columns 1 and 4 for both V and H data. There are two possible causes which could account for this difference: 1) the effects of the ionosphere on the polarization rotation, and 2) the effects of variations in spacecraft attitude. It unlikely that this difference is attributable to the ionosphere since all of the data within this run comes from night passes, when the Faraday rotation ionosphere effect is minimal. However, all of the GOASEX passes have attitude variations from north to south of about 0.2°. This change in attitude could result in polarization rotation changes which affect the outer cells (1 and 4) more than the inner cells (2 and 3). Further study would be required to determine if this is indeed the case.

3.4.2 Discussion of Runs 3, 5, 7, and 8. These four runs are the components which when combined make up RUN 10. In general, each run in this set exhibits those characteristics enumerated above for RUN 10. The following observations are made regarding the individual runs:

(a) The curve fits for RUN 7 exhibit more pronounced deviation from the model curves than do those of the other runs. This is due to the fact that data is available only for a very narrow range of SST. However, within the range where data is available, the data points fall along a biased model curve very well. This can be seen from the RMS values for each column, which are smaller than the corresponding values for RUN 10 in almost every case.

(b) Runs 3 and 5 exhibit more upward scatter in the data than do Runs 7 and 8. This might be attributable to rain and/or high winds.

3.4.3 Discussion of Runs 6 and 9 — Sidelobe Effects. RUN 6 consists of the two ascending GOASEX passes which closely parallel the North American west coast. RUN 9 combines all of the RUN 10 data with that of RUN 6. The following observations are made regarding these two runs:

(a) The data from RUN 6 includes sidelobe effects from the North American west coast. Column 4 data is affected most strongly since it represents the part of the SMMR swath closest to shore. In comparison with the RUN 10 data, all of the data for RUN 6 appears to be biased in the direction of increasing T_B by about 5°K. This phenomenon appears in the statistics for

RUN 6 as large positive biases about the model curves for both V and H data and as larger RMS values than are observed in other runs. However, it is not known how much of this effect is due to sidelobes and how much is due to high winds which were probably present for orbit 1212 of this run.

(b) The spurious points from the RUN 6 data blocks cause the RMS values of RUN 9 to exceed those of RUN 10, and also shift the RUN 9 biases above those of RUN 10.

3.4.4 Discussion of RUN 4 Vs. RUN 3 — Rain Effects. RUN 4 contains the same data as RUN 3 except that three blocks containing suspected rain cells are omitted. This results in less data scatter (particularly for H data) and in downward shifted biases (again, particularly for H data). However, it is not known how much of this effect is due to rain and how much is due to local high winds associated with the rain cells.

As previously noted in Section 3.4.2, runs 3 and 5 show more upward data scatter than do runs 7 and 8. RUN 4 resembles Runs 7 and 8 in terms of data scatter, implying that Runs 7 and 8 probably contain less rain than do Runs 3 and 5.

3.4.5 Discussion of Runs 11 through 14. This section discusses the results of two supplementary studies which we performed in order to investigate possible origins of the cross-track gradient found in the T_B data. Each of the two programs developed for these supplementary studies was run for four individual GOASEX passes as shown in Table 2. The following observations are made regarding runs 11 through 14:

(a) As shown in Figures 11.2 through 14.2, there is no obvious correspondence between ΔT_B and incidence angle. Since incidence angle is determined by spacecraft attitude, this seems to imply that no obvious relation exists between ΔT_B and attitude.

(b) Figures 11.1 through 14.1 verify the principal study result that in general, the V and H cross-track gradients are in opposite directions, i.e., that the vertical T_B gradient from column 1 to column 4 is usually positive and the H gradient is usually negative. In addition, the magnitude of the H gradient is usually larger than that of the V gradient.

(c) The cross-track gradients do not seem to show any strong dependence on latitude.

(d) The cross-track gradients for V and H data seem to be correlated with each other in the sense that when the V gradient increases (decreases) in value, the H gradient also increases (decreases). However, the H gradient appears to show larger variations than does the V gradient.

(e) RUN 14 is corrupted by extensive sidelobe effects near latitudes of 38°N (California coast) and 51°N (Queen Charlotte Island).

(f) The observed variations in the T_B gradients are very difficult to explain in some cases. Some of these variations are possibly due to strong wind-speed gradients across the SMMR swath. However, it is puzzling that for the cases run, most of the gradient variations for both V and H appear to be only in the positive direction. Further study would be required to determine the factors causing these gradient variations.

3.4.6 Discussion of T_A Data Survey. This section discusses the results of the third supplementary study, which we performed to determine if the T_B gradients have their origin in the input T_A data. We surveyed T_A data from three GOASEX passes in order to determine the position within the SMMR scan at which the minimum polarization rotation effect occurs. Assuming a constant scene temperature, the vertical T_A values should reach a maximum and the horizontal T_A values should reach a minimum at this scan position of minimum polarization rotation. This is expected to occur at the center of the scan where the scan angle is equal to zero. For the 6.6 GHz data, the scan center occurs at footprint number 9 out of 16 samples for each scan. The results of our brief survey are shown in Table 15.

Although these results are by no means conclusive, several points should be noted.

(a) The data chosen for the survey represents time periods during which the T_B data exhibit strong cross-track gradients as previously discussed in section 3.4.5. In particular, the horizontal T_B data exhibit large negative gradients, while the vertical data exhibit positive gradients of smaller magnitude.

(b) For all three passes considered the mean scan position of minimum polarization rotation for H data is always greater than 9, while that for V data is always less than 9. In addition, the mean H scan position always differs from 9 by a larger amount than does the V mean position. Although no firm conclusion may be drawn, the directions and relative magnitudes of these discrepancies qualitatively agree with the directions and relative magnitudes of the observed T_B cross-track gradients. This suggests that a more rigorous investigation of the T_A data might reveal the source of the T_B biases.

4.0 CONCLUSIONS

Several conclusions may be drawn from the results discussed in the previous section 3.4:

(1) There appear to exist opposing cross-track gradients in the V and H 6.6 GHz brightness temperatures output by the interim APC

algorithm. These gradients are opposing in the sense that the vertical T_B values tend to increase across the SMMR swath from cell number 1 to cell number 4, whereas the horizontal T_B values tend to decrease. The magnitude of the change across the swath is greater for H data (about 3°K) than for V data (about 1.5°K).

(2) For both V and H data, the T_B values for cell number 4 appear to agree best with model-predicted T_B values. In addition, the T_B data shows progressively less agreement with the models as one moves from cell 4 to cell 1 data. This effect is illustrated best by the bias values given in Table 10 (-0.78 to -2.31°K for V and 0.55 to 3.45°K for H). However, these biases for V and H include unknown positive environmental biases due to the effects of high winds, clouds, and rain. These unknown environmental biases for V and H should be subtracted from the biases in Table 10 to arrive at the true instrument biases. Therefore, it may very well be true that the actual instrument biases for both V and H are negative, with V more strongly biased than H.

(3) If the observed biases are removed from the measured T_B data, the resulting values agree quite well with model-predicted values. This is best illustrated by the RMS dispersions shown in Table 10. The dispersion of all the V data about the biased model curve is 1.5°K while that of the H data is 2.6°K. These exceed the dispersions about the least-squares fitted curves by only 10%.

(4) In agreement with model predictions, the H data appears to be twice as sensitive to wind speed variations as the V data. This is evidenced by the larger degree of scatter found in the H data.

(5) As expected, nearby land does corrupt SMMR data through sidelobe contributions. These effects must be removed in order to successfully make use of coastal SMMR data.

(6) There does not appear to be any obvious correlation between the observed T_B cross-track gradients and incidence angle, which implies that the T_B gradients are independent of spacecraft attitude.

(7) There does not appear to be any strong relationship between the T_B cross-track gradients and latitude. However, some of the observed variations in T_B gradients are not currently understood.

(8) A brief survey of the T_A data suggests that the origin of the T_B cross-track gradients may lie within the T_A values. However, a much more rigorous investigation would be needed to confirm this hypothesis.

5.0 RECOMMENDATIONS

As a result of this study, we feel that the following recommendations are appropriate.

(1) The implementation of the final APC algorithm should be completed. Upon completion, several runs made for this study should be repeated using T_B data from the final APC. This will allow a determination of whether the sidelobe contributions have been successfully removed, and whether the cross-track gradients are still apparent.

(2) If the T_B cross-track gradients are still observable in the final APC output, it is recommended that a detailed analysis of the T_A input data be performed to determine what is causing the gradients.

(3) In order to further refine estimates of the observed instrument biases, it is recommended that this analysis be extended to include data obtained under low wind-speed, extremely clear weather conditions. This will require the use of non-GOASEX data as it becomes available. Furthermore, additional insight into the nature of the T_B cross-track gradients will be gained by analyzing good ascending passes as well as descending passes.

6.0 NEW TECHNOLOGY

No new technology has been developed in the course of this study.

7.0 REFERENCES

Acknowledgement should be given to three general sources of information used for this study.

(1) Njoku, E. G. "Antenna Pattern Correction Procedures for the Scanning Multichannel Microwave Radiometer (SMMR)," JPL Publication.

(2) NOAA National Marine Fisheries Services (NMFS) (1978). Fishing Information, No. 9.

(3) "Seasat Gulf of Alask Workshop Report," Volumes 1 and 2, JPL Publication 622-101.

Table 1. SMMR APC Brightness Temperature Grids

Grid Number	Grid Size (cells)	Cell Dimension (km)	SMMR Channels Output on Grid	
1	4 x 4	149 x 149	6.6 V	6.6 H
			10.69 V	10.69 H
			18 V	18 H
			21 V	21 H
			37 V	37 H
2	7 x 7	85 x 85	10.69 V	10.69 H
			18 V	18 H
			21 V	21 H
			37 V	37 H
3	11 x 11	54 x 54	18 V	18 H
			21 V	21 H
			37 V	37 H
4	22 x 22	27 x 27	37 V	37 H

Figure 1. 6.6 GHz Standard Atmosphere — Low Wind Speed Reference Curves

$$T_{B_{VERT}} = 321.678 - 1.71645\,T_s + 0.00389942\,T_s^2$$

$$T_{B_{HORI}} = 218.208 - 1.21228\,T_s + 0.00258746\,T_s^2$$

where

T_s = sea surface temperature

T_B = model — predicted 6.6 GHz brightness temperature for the appropriate polarization

for the following assumptions:

1) Standard atmosphere model

2) Integrated water vapor content of 2.4 g/cm^2

3) Wind speed between 0 and 7 m/sec.

4) Cloud-free conditions

Figure 2.1

NMFS Mean Sea Surface Temperature Map for September, 1978

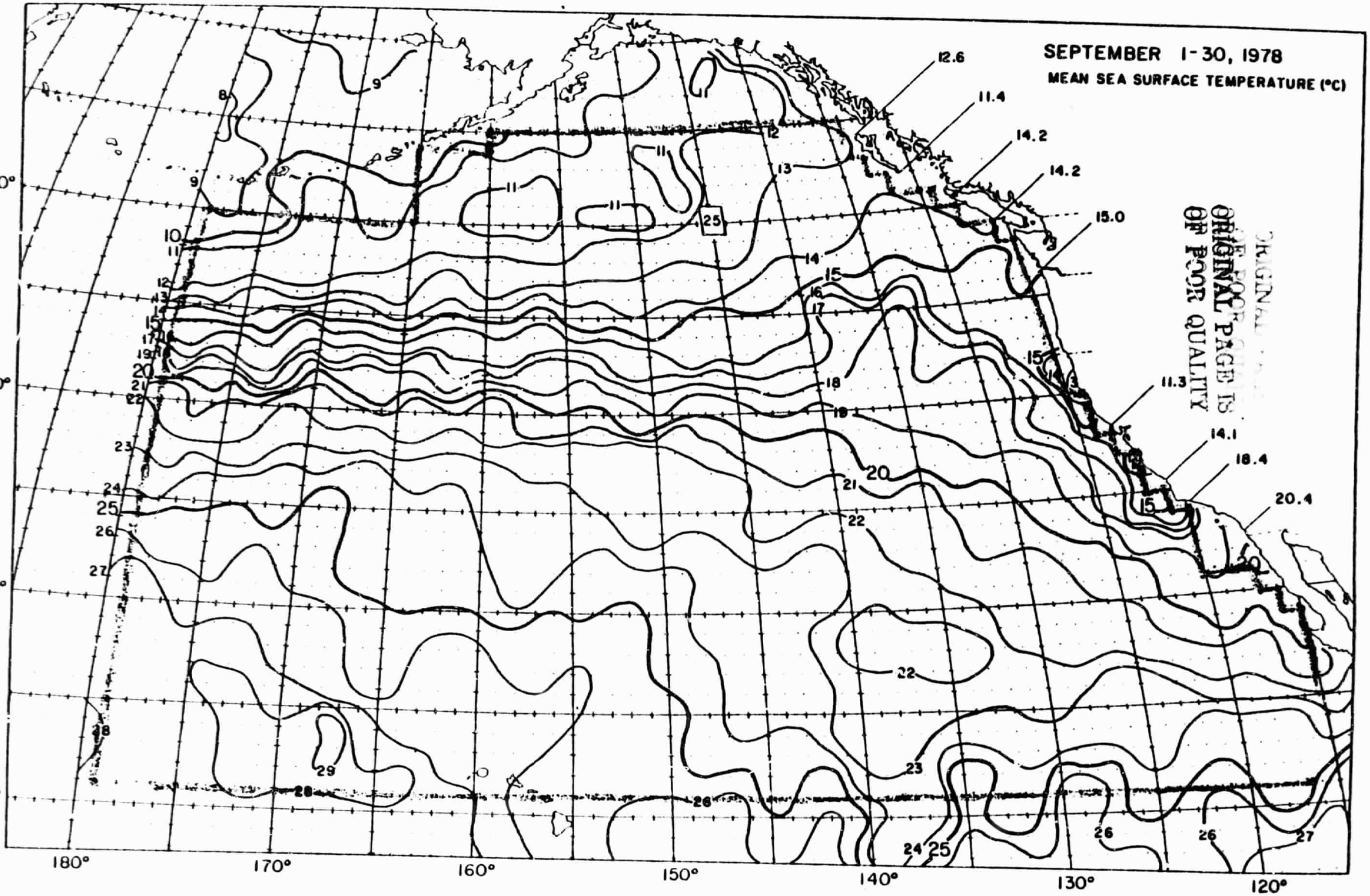

Figure 2.2

Resulting SST Contour Map Produced from Digitized NMFS Map

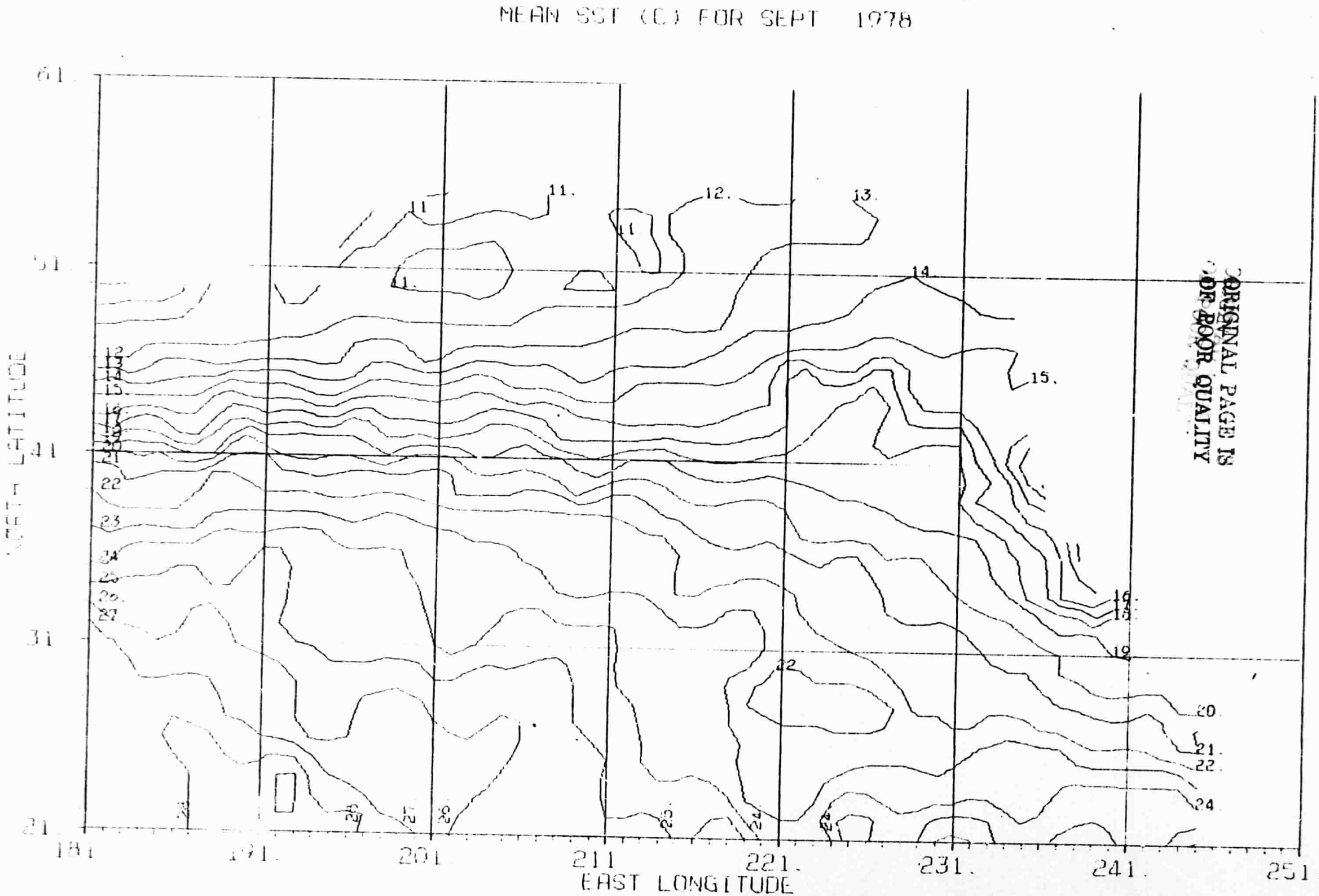

Table 2. Summary of Runs (Page 1 of 3)

Run I.D.	Run Type	SEASAT-A Orbit No.	Start Time	Stop Time	No. of Blocks	Comments
RUN1	A	1298	268,18,28,11	268,18,29,41	1	Test Case
RUN2	A	1298	268,18,26,40	268,18,29,41	2	Test Case
RUN3	A	1293	268,10,31,42	268,10,39,11	5	Descending Orbits. Orbits 1293 and 1164 probably include rain. Orbits 1293 and 1207 probably include high winds, particularly at higher latitudes.
		1164	259, 9,53,41	259,10, 1,11	5	
		1207	262,10, 5,41	262,10,14,42	6	
					16	
RUN4	A	1293	268,10,31,42	268,10,34,42	2	This run duplicates RUN3 except that 3 blocks which probably contain rain were omitted.
		1293	268,10,36,11	268,10,39,11	2	
		1164	259, 9,53,41	259, 9,55,11	1	
		1164	259, 9,58,11	259,10, 1,11	2	
		1207	262,10, 5,41	262,10,14,42	6	
					13	
RUN5	A	1292	268, 8,51,41	268, 8,59,11	5	Descending orbits. Orbit 1292 probably includes rain. All 3 orbits contain high winds, especially 1292.
		1163	259, 8,13,40	259, 8,20,11	5	
		1206	262, 8,26,42	262, 8,34,13	5	
					15	
RUN6	A	1298	268,18,26,40	268,18,29,41	2	Ascending orbits. Sidelobe effects in both orbits. Suspected EMI in orbit 1298. Orbit 1212 probably includes high winds.
		1298	268,18,32, 7	268,18,36,37	3	
		1212	262,18, 2,11	262,18,11,11	6	
					11	
RUN7	A	1177	260, 7,46,40	260, 7,52,40	4	Descending orbits. Orbit 1177 probably contains wind speeds somewhat higher than 7 m/sec. (~ 10 m/sec.)
		1134	257, 7,33,42	257, 7,39,42	4	
					8	

Table 2. Summary of Runs (Page 2 of 3)

Run I.D.	Run Type	SEASAT-A Orbit No.	Start Time	Stop Time	No. of Blocks	Comments
RUN8	A	1135	257, 9,11,40	257, 9,19,10	5	Descending orbits. Orbit 1135 probably contains rain and high winds. Orbit 1178 probably contains some high winds.
		1178	260, 9,23,40	260, 9,32,41	6	
					11	
RUN9	A	1293	268,10,31,42	268,10,39,11	5	This run combines the data from Runs 3, 5, 6, 7, and 8. This includes all usable GOASEX data. No attempt was made to exclude bad data.
		1164	259, 9,53,41	259,10, 1,11	5	
		1207	262,10, 5,41	262,10,14,42	6	
		1292	268, 8,51,41	268, 8,59,11	5	
		1163	259, 8,13,40	259, 8,20,11	5	
		1206	262, 8,26,42	262, 8,34,13	5	
		1298	268,18,26,40	268,18,29,41	2	
		1298	268,18,32, 7	268,18,36,37	3	
		1212	262,18, 2,11	262,18,11,11	6	
		1177	260, 7,46,40	260, 7,52,40	4	
		1134	257, 7,33,42	257, 7,39,42	4	
		1135	257, 9,11,40	257, 9,19,10	5	
		1178	260, 9,23,40	260, 9,32,41	6	
					61	
RUN10	A	1293	268,10,31,42	268,10,39,11	5	This run combines the data from Runs 3, 5, 7, and 8. This run duplicates RUN9 except that sidelobe-corrupted RUN6 was omitted.
		1164	259, 9,53,41	259,10, 1,11	5	
		1207	262,10, 5,41	262,10,14,42	6	
		1292	268, 8,51,41	268, 8,59,11	5	
		1163	259, 8,13,40	259, 8,20,11	5	
		1206	262, 8,26,42	262, 8,34,13	5	
		1177	260, 7,46,40	260, 7,52,40	4	
		1134	257, 7,33,42	257, 7,39,42	4	
		1135	257, 9,11,40	257, 9,19,10	5	
		1178	260, 9,23,40	260, 9,32,41	6	
					50	

Table 2. Summary of Runs (Page 3 of 3)

Run I.D.	Run Type	SEASAT-A Orbit No.	Start Time	Stop Time	No. of Blocks	Comments
RUN11-1	B	1135	257, 9,11,40	257, 9,19,10	5	One orbit from RUN8
RUN11-2	C	1135	257, 9,11,40	257, 9,19,10	5	One orbit from RUN8
RUN12-1	B	1206	262, 8,26,42	262, 8,34,13	5	One orbit from RUN5
RUN12-2	C	1206	262, 8,26,42	262, 8,34,13	5	One orbit from RUN5
RUN13-1	B	1207	262,10, 5,41	262,10,14,42	6	One orbit from RUN3
RUN13-2	C	1207	262,10, 5,41	262,10,14,42	6	One orbit from RUN3
RUN14-1	B	1212	262,18, 2,11	262,18,11,11	6	One orbit from RUN6
RUN14-2	C	1212	262,18, 2,11	262,18,11,11	6	One orbit from RUN6

Run Type Definitions:

A - T_B vs. SST Plots and Statistics

B - Cross-track Gradient vs. Latitude

C - T_B Minus Model T_B vs. Incidence Angle

Times are in Days, Hours, Minutes, Seconds from beginning of year 1978.

Table 3.

RUN 3 Statistical Summary

CURVE FITS FOR SMMR 6.6 GHZ VERSUS SST

COLUMN	CONSTANT TERM	LINEAR TERM	QUADRATIC TERM	RMS
1 V	1768.76	-11.60	.0207	1.112
2 V	1402.67	-9.04	.0163	1.075
3 V	763.84	-4.62	.0086	1.127
4 V	25.43	.43	.0000	1.351
ALL V	1269.46	-8.11	.0147	1.341
1 H	2107.40	-14.10	.0246	2.081
2 H	1154.21	-7.49	.0132	1.649
3 H	63.65	.08	.0000	1.849
4 H	68.34	.06	.0000	2.263
ALL H	44.39	.15	.0000	2.259

DISPERSION ABOUT STANDARD ATMOSPHERE - LOW WIND SPEED CURVE

COLUMN	BIAS	RMS
1 V	-2.96	1.203
2 V	-1.89	1.249
3 V	-1.61	1.413
4 V	-1.20	1.564
ALL V	-1.91	1.512
1 H	2.78	2.142
2 H	2.66	1.792
3 H	1.88	2.277
4 H	.51	2.726
ALL H	1.96	2.434

Figure 3.1

RUN 3

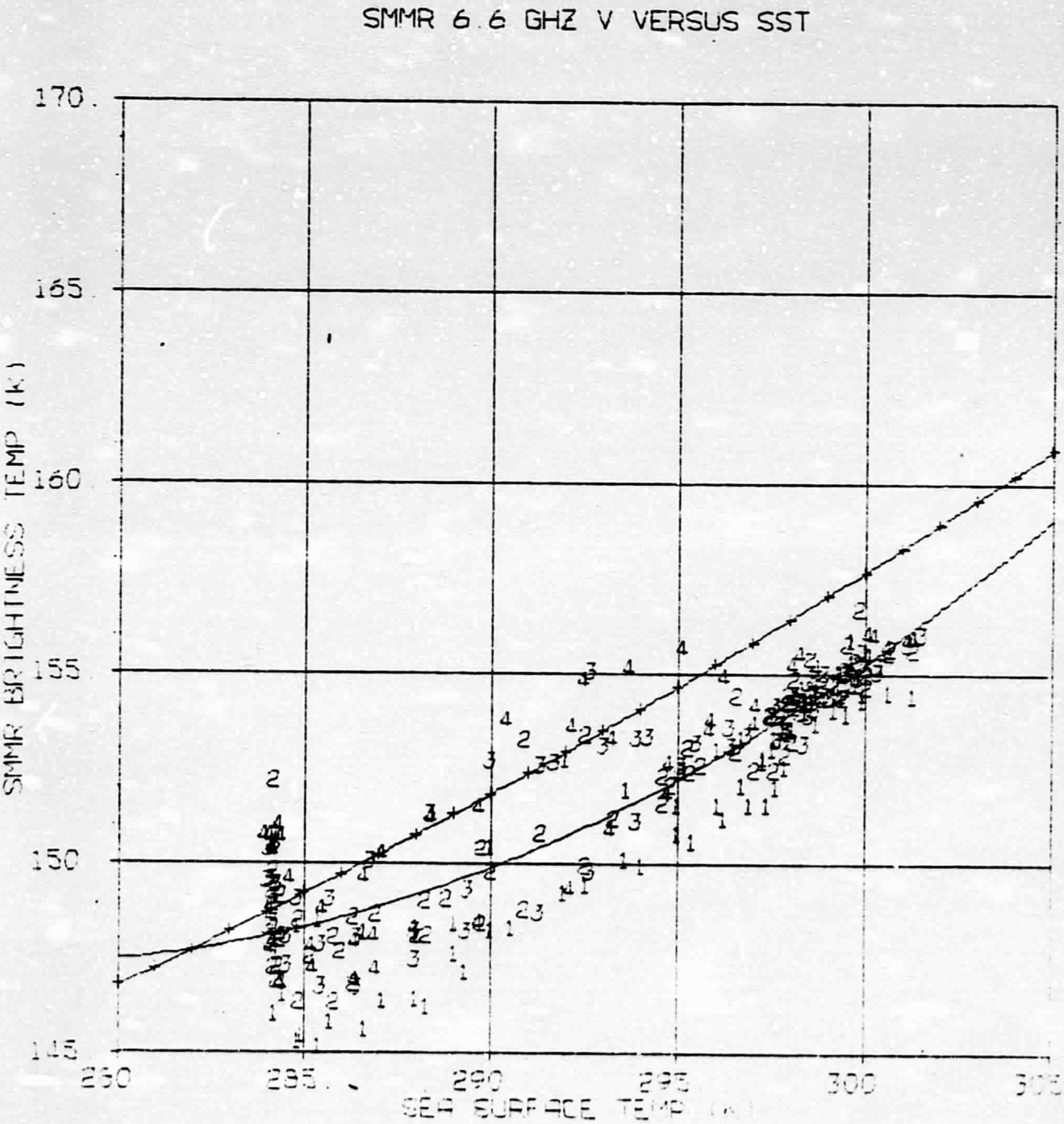

Figure 3.2

RUN 3 Curve Fits for

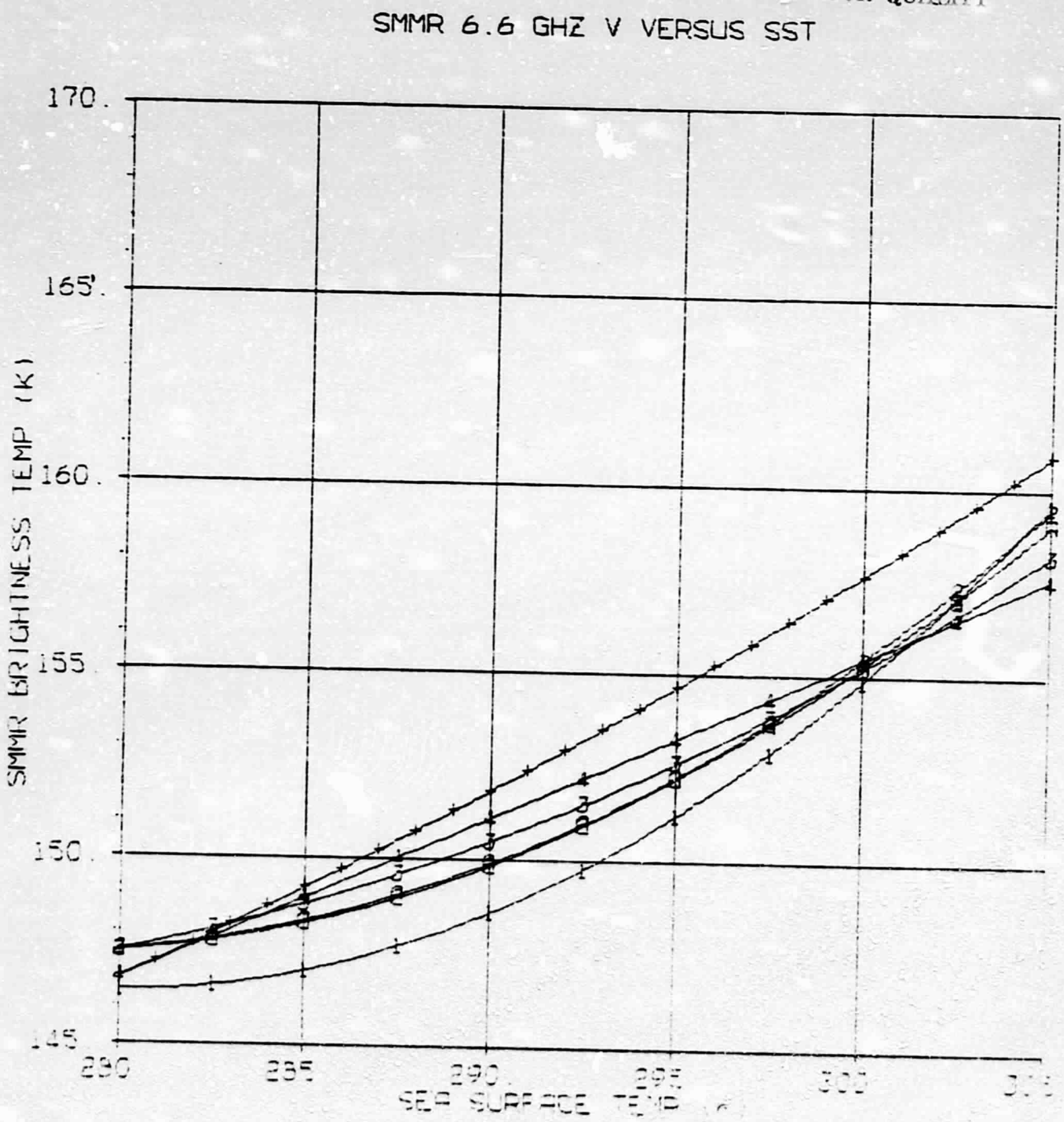

Figure 3.3

RUN 3

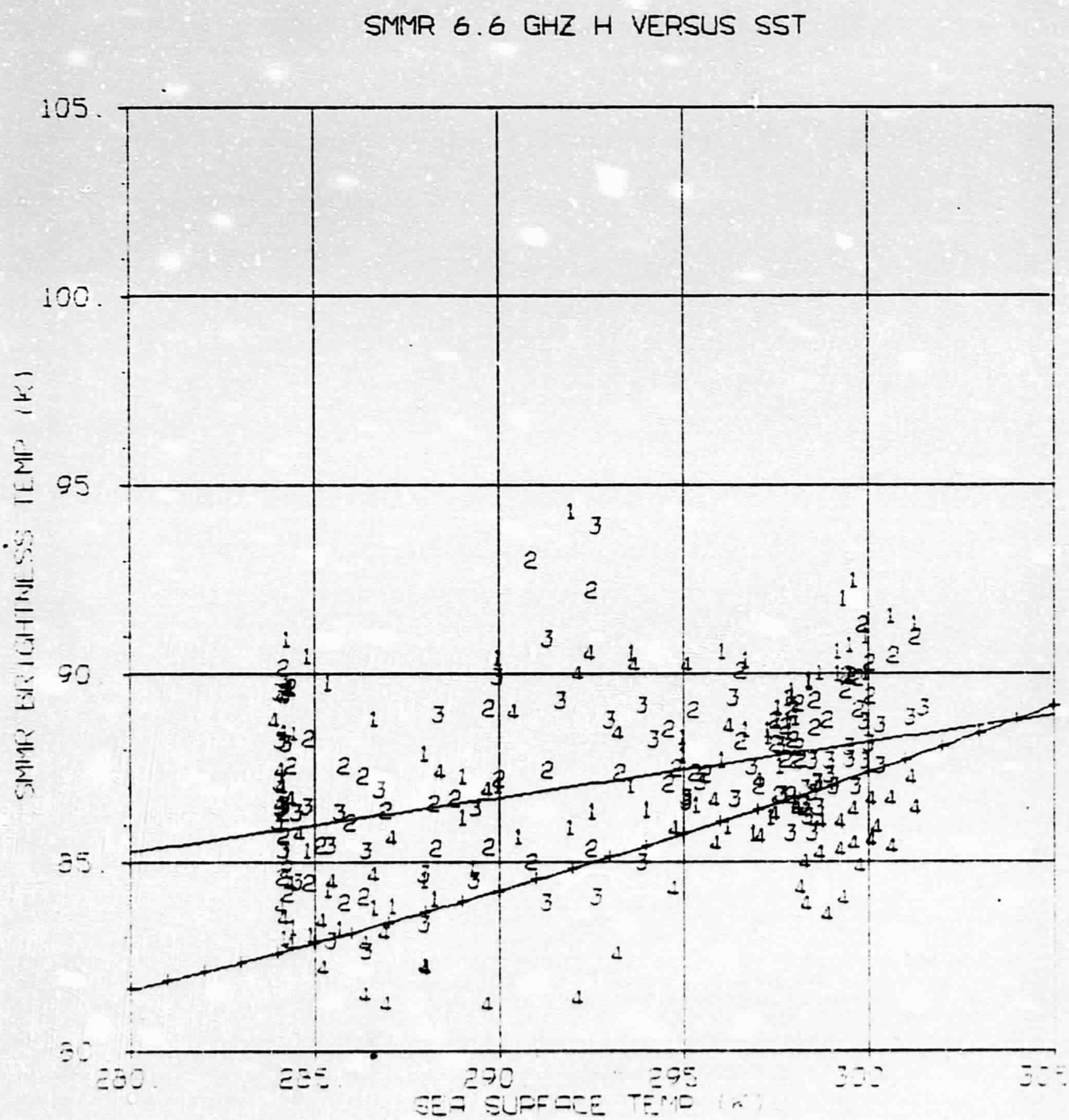

Figure 3.4

RUN 3 Curve Fits for

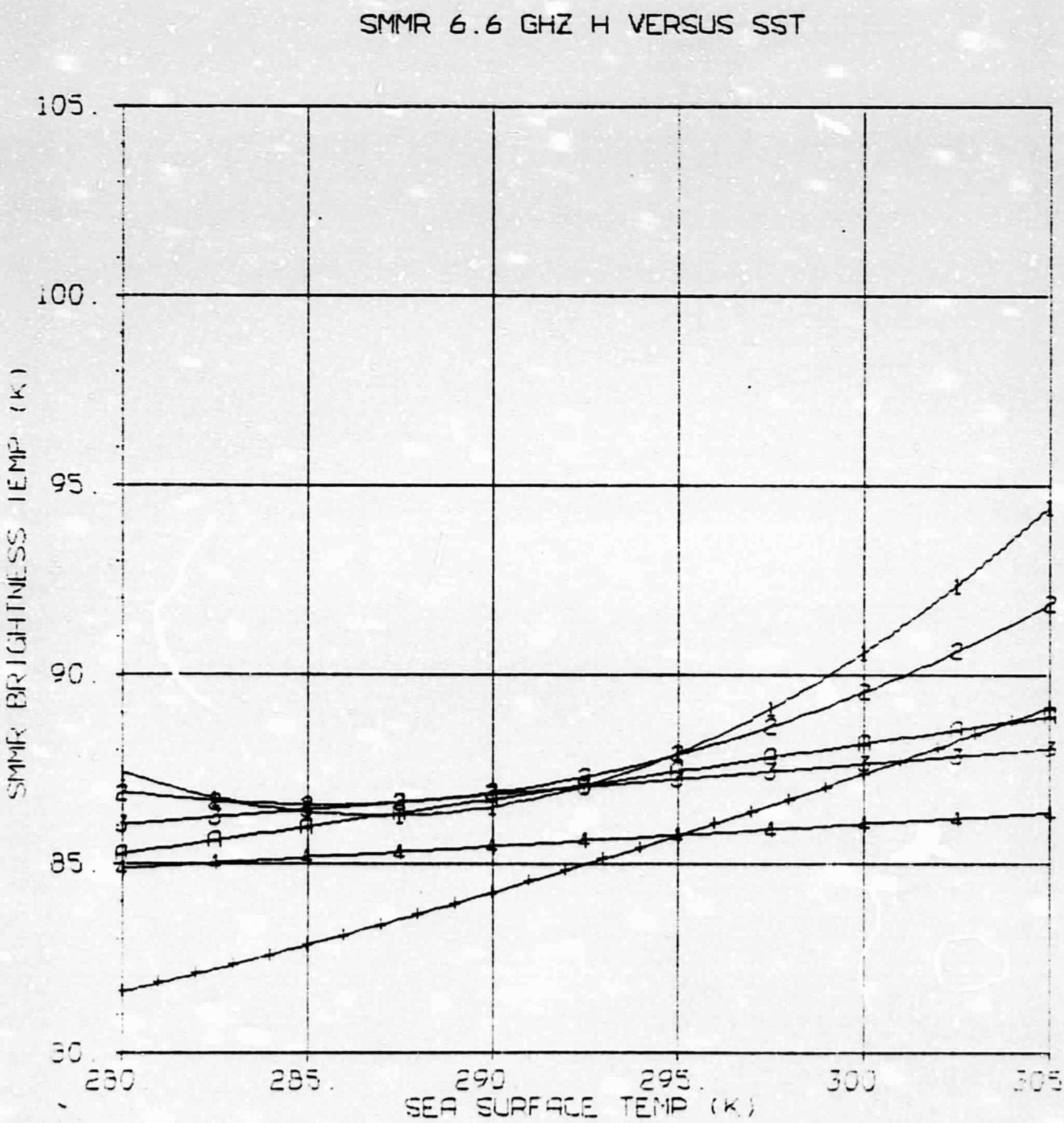

Table 4.

RUN 4 Statistical Summary

CURVE FITS FOR SMMR 6.6 GHZ VERSUS SST

COLUMN	CONSTANT TERM	LINEAR TERM	QUADRATIC TERM	RMS
1 V	2204.13	-14.58	.0258	1.052
2 V	2301.21	-15.19	.0268	.990
3 V	1964.90	-12.83	.0227	.898
4 V	2144.75	-14.07	.0248	1.023
ALL V	2423.80	-16.02	.0282	1.140
1 H	3347.33	-22.60	.0392	1.850
2 H	2924.51	-19.63	.0339	1.312
3 H	2334.77	-15.47	.0266	1.367
4 H	3015.57	-20.11	.0345	1.718
ALL H	2307.96	-15.35	.0265	2.034

DISPERSION ABOUT STANDARD ATMOSPHERE - LOW WIND SPEED CURVE

COLUMN	BIAS	RMS
1 V	-2.89	1.174
2 V	-1.90	1.266
3 V	-1.69	1.397
4 V	-1.36	1.475
ALL V	-1.96	1.450
1 H	2.79	1.992
2 H	2.55	1.617
3 H	1.66	2.110
4 H	.15	2.557
ALL H	1.79	2.339

Figure 4.1

RUN 4

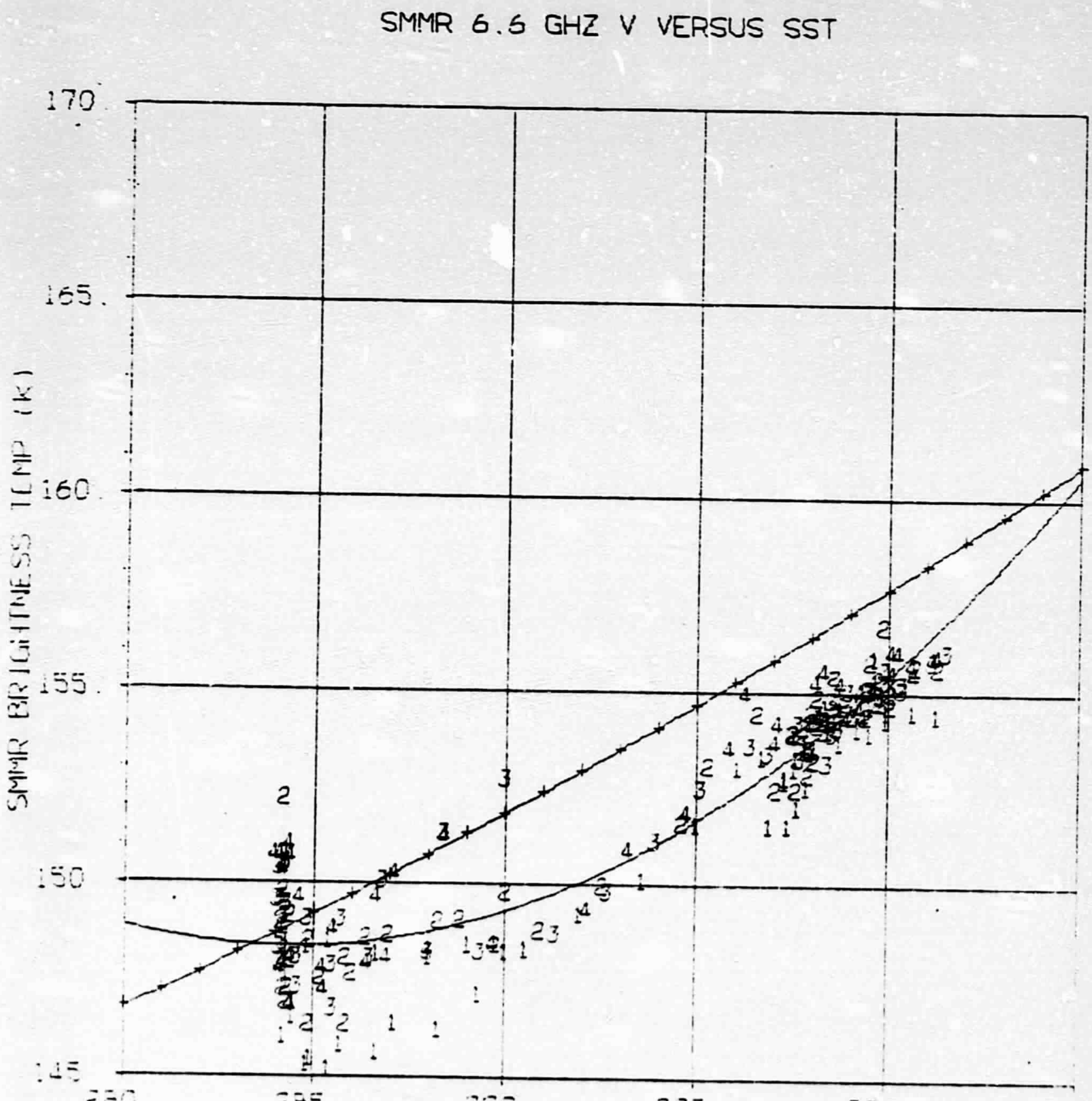

Figure 4.2

RUN 4 Curve Fits for

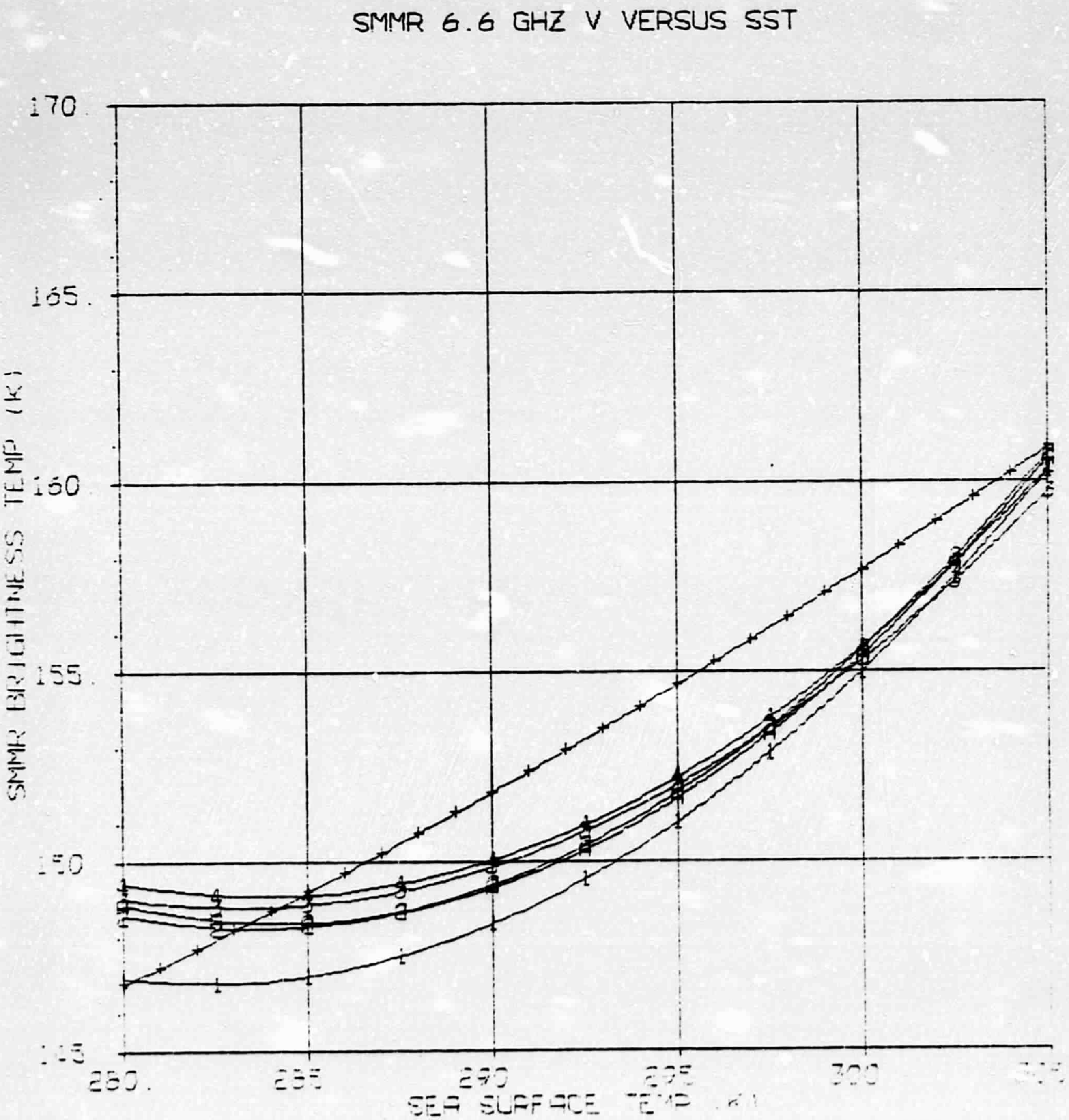

Figure 4.3

RUN 4

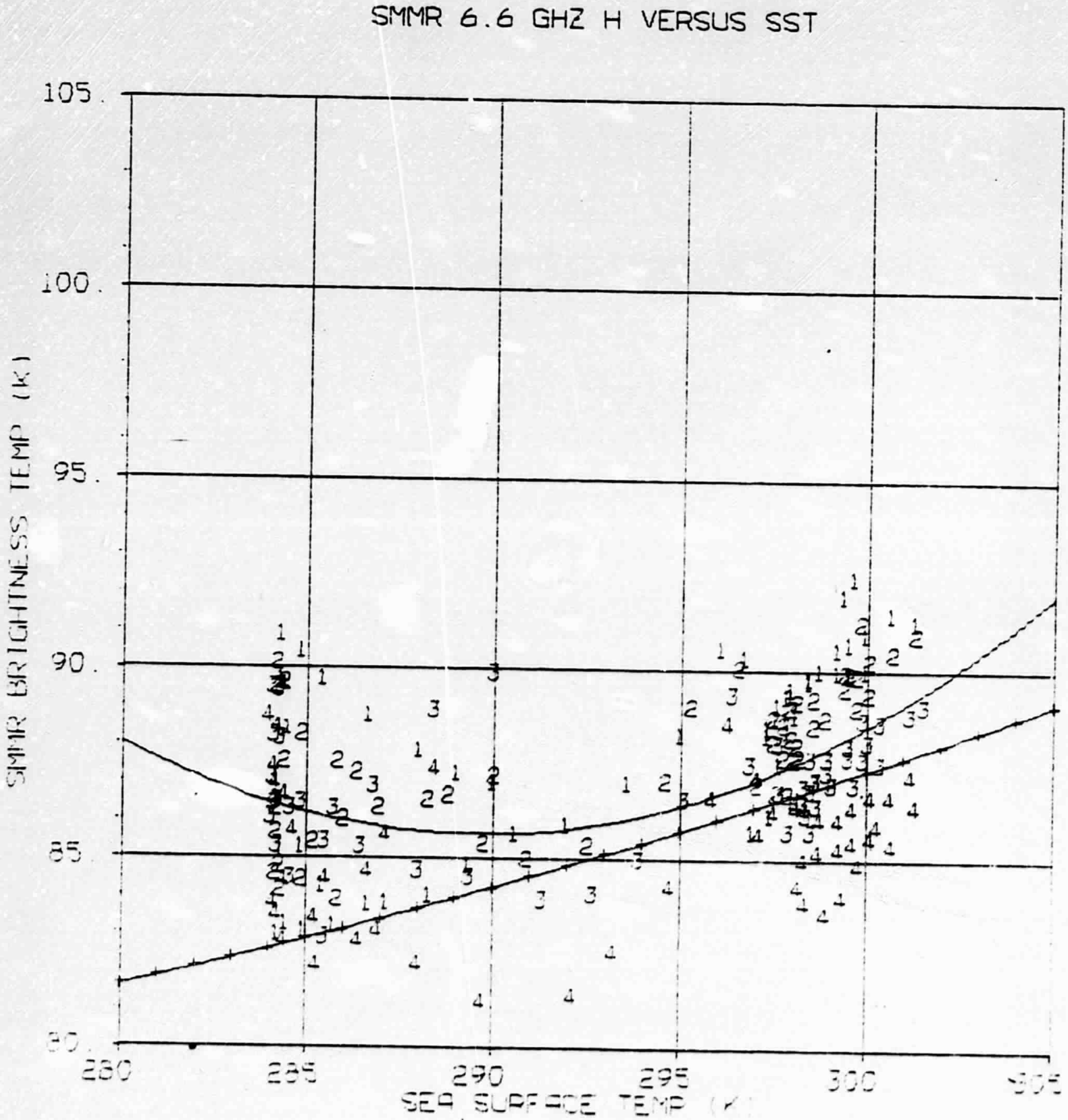

Figure 4.4

RUN 4 Curve Fits for

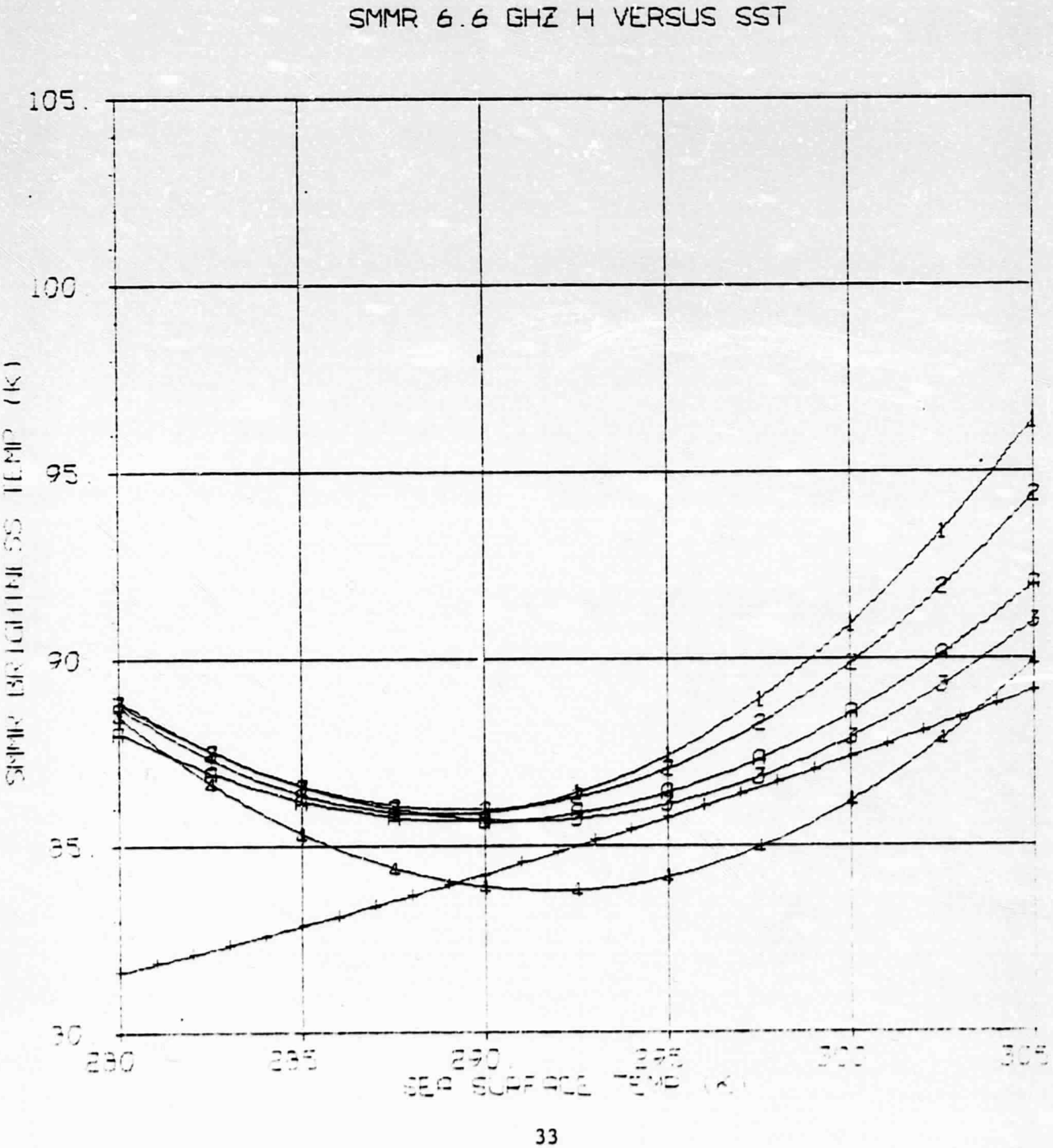

Table 5.

RUN 5 Statistical Summary

CURVE FITS FOR SMMR 6.6 GHZ VERSUS SST

COLUMN		CONSTANT TERM	LINEAR TERM	QUADRATIC TERM	RMS
1	V	20.30	.45	.0000	1.394
2	V	3979.05	-26.46	.0457	1.225
3	V	5096.11	-34.08	.0587	1.207
4	V	2439.82	-15.85	.0275	1.556
ALL	V	4388.56	-29.24	.0504	1.473
1	H	4690.72	-31.74	.0547	2.519
2	H	7497.91	-50.66	.0866	2.203
3	H	11332.21	-76.80	.1311	2.158
4	H	5247.39	-35.12	.0597	2.509
ALL	H	5322.10	-35.80	.0612	2.728

DISPERSION ABOUT STANDARD ATMOSPHERE - LOW WIND SPEED CURVE

COLUMN		BIAS	RMS
1	V	-1.94	1.434
2	V	-1.35	1.444
3	V	-.98	1.558
4	V	-.18	1.999
ALL	V	-1.11	1.745
1	H	4.08	2.548
2	H	3.41	2.384
3	H	2.28	2.655
4	H	1.18	3.052
ALL	H	2.74	2.870

Figure 5.1

RUN 5

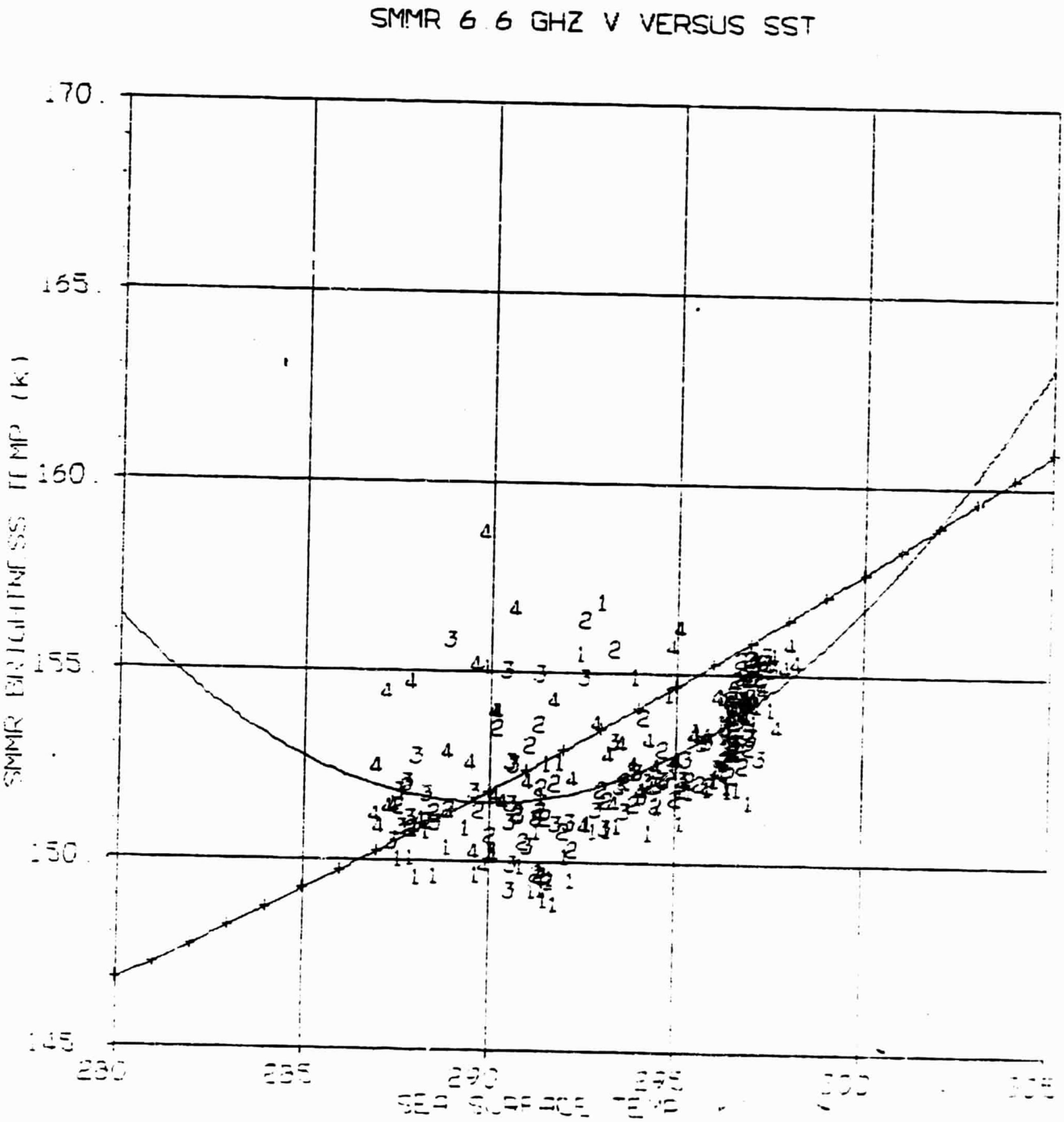

Figure 5.2

RUN 5 Curve Fits for

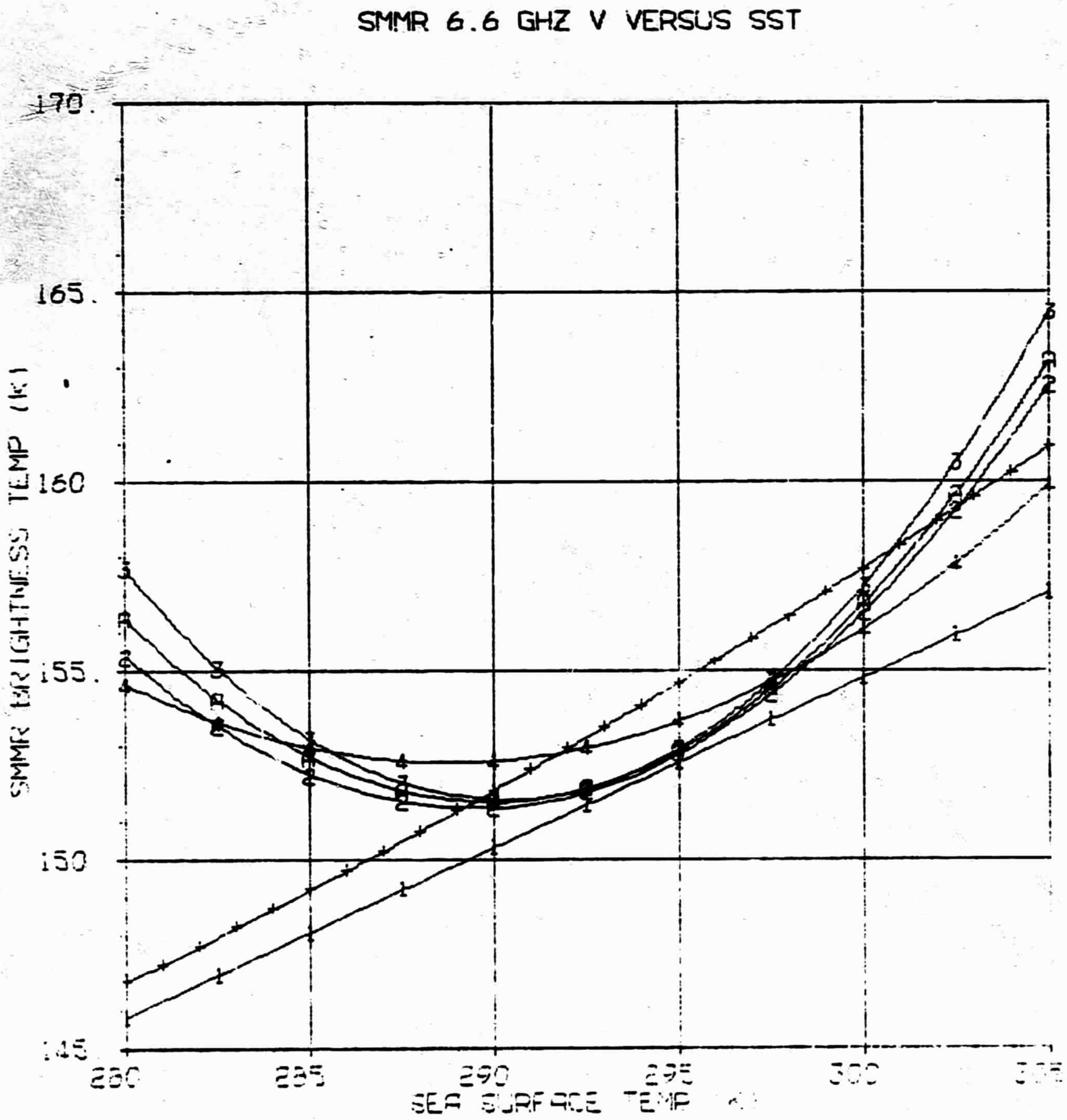

Figure 5.3

RUN 5

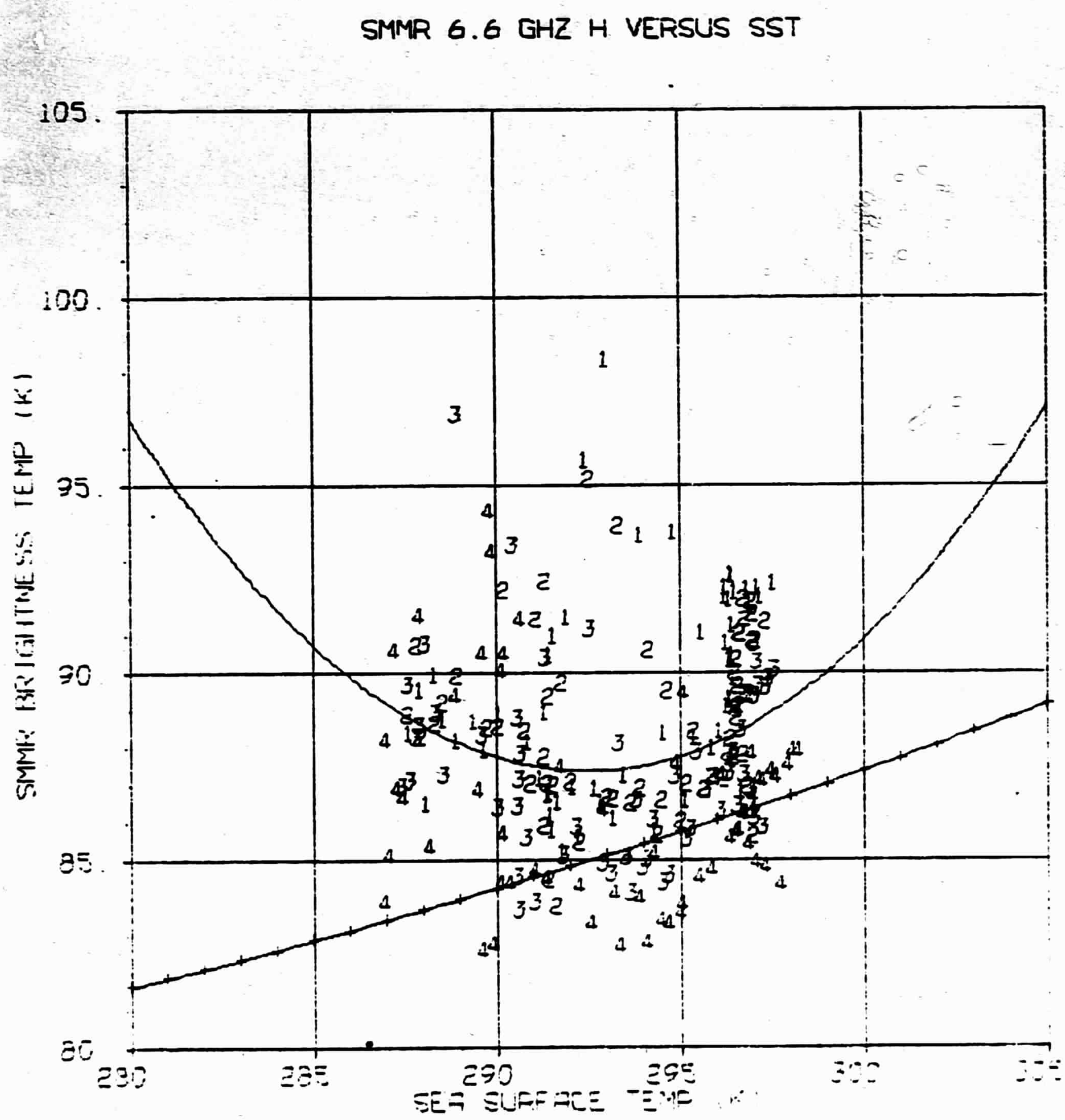

Figure 5.4

RUN 5 Curve Fits for

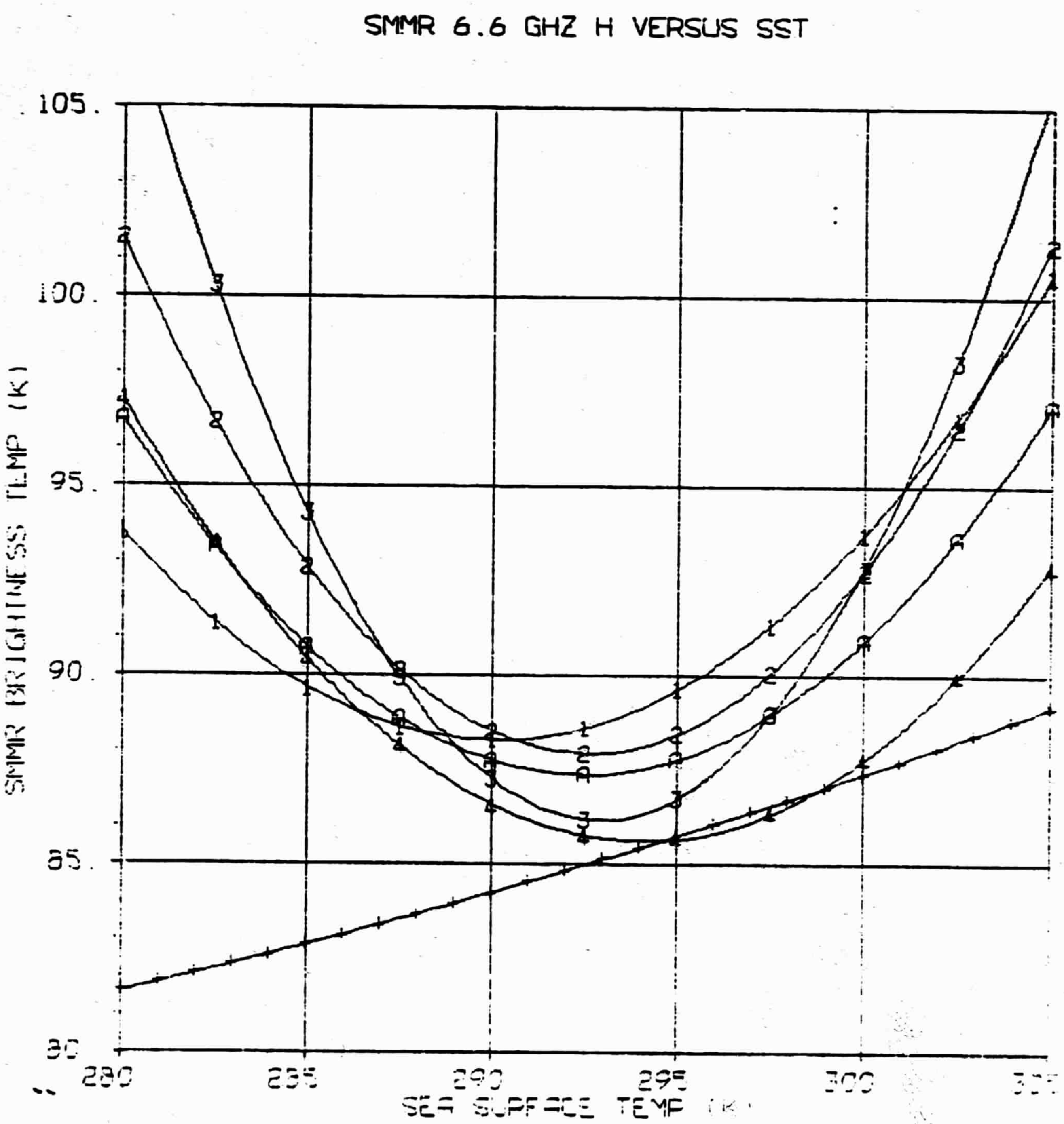

Table 6.

RUN 6 Statistical Summary

CURVE FITS FOR SMMR 6.6 GHZ VERSUS SST

COLUMN		CONSTANT TERM	LINEAR TERM	QUADRATIC TERM	RMS
1	V	122.74	.11	.0000	1.909
2	V	6929.87	-47.05	.0817	3.659
3	V	15108.83	-103.51	.1791	5.521
4	V	10702.41	-72.67	.1252	2.708
ALL	V	6350.52	-42.89	.0742	4.118
1	H	-2834.56	20.58	-.0362	2.663
2	H	-3682.43	26.40	-.0462	1.906
3	H	17824.80	-122.12	.2102	7.254
4	H	14937.22	-101.05	.1719	5.646
ALL	H	4221.55	-27.99	.0474	5.406

DISPERSION ABOUT STANDARD ATMOSPHERE - LOW WIND SPEED CURVE

COLUMN		BIAS	RMS
1	V	1.41	2.506
2	V	3.10	3.782
3	V	4.45	5.961
4	V	4.51	3.096
ALL	V	3.37	4.245
1	H	6.87	3.976
2	H	7.53	3.385
3	H	8.33	7.639
4	H	6.04	7.026
ALL	H	7.19	5.870

Figure 6.1

RUN 6

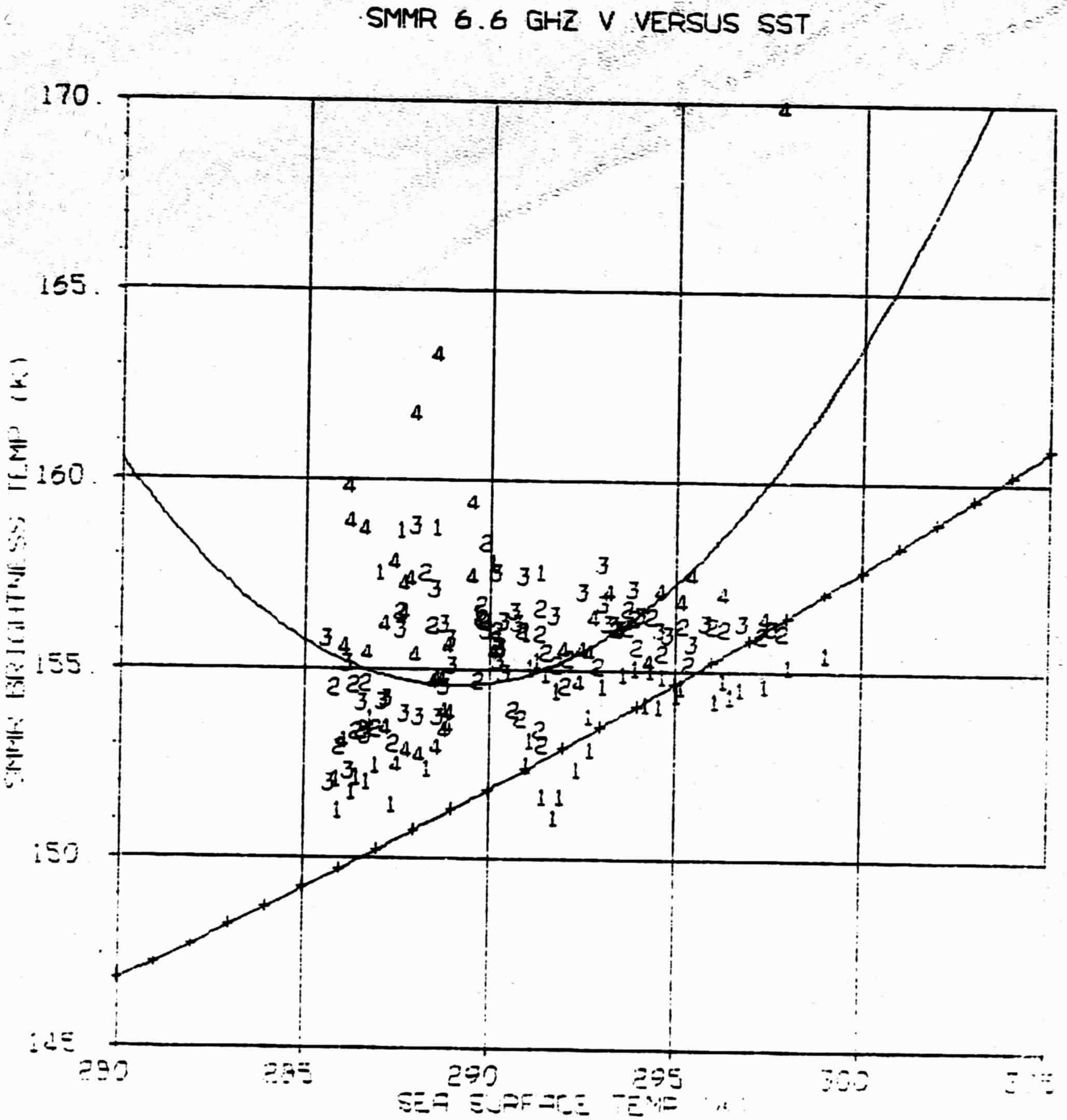

Figure 6.2

RUN 6 Curve Fits for

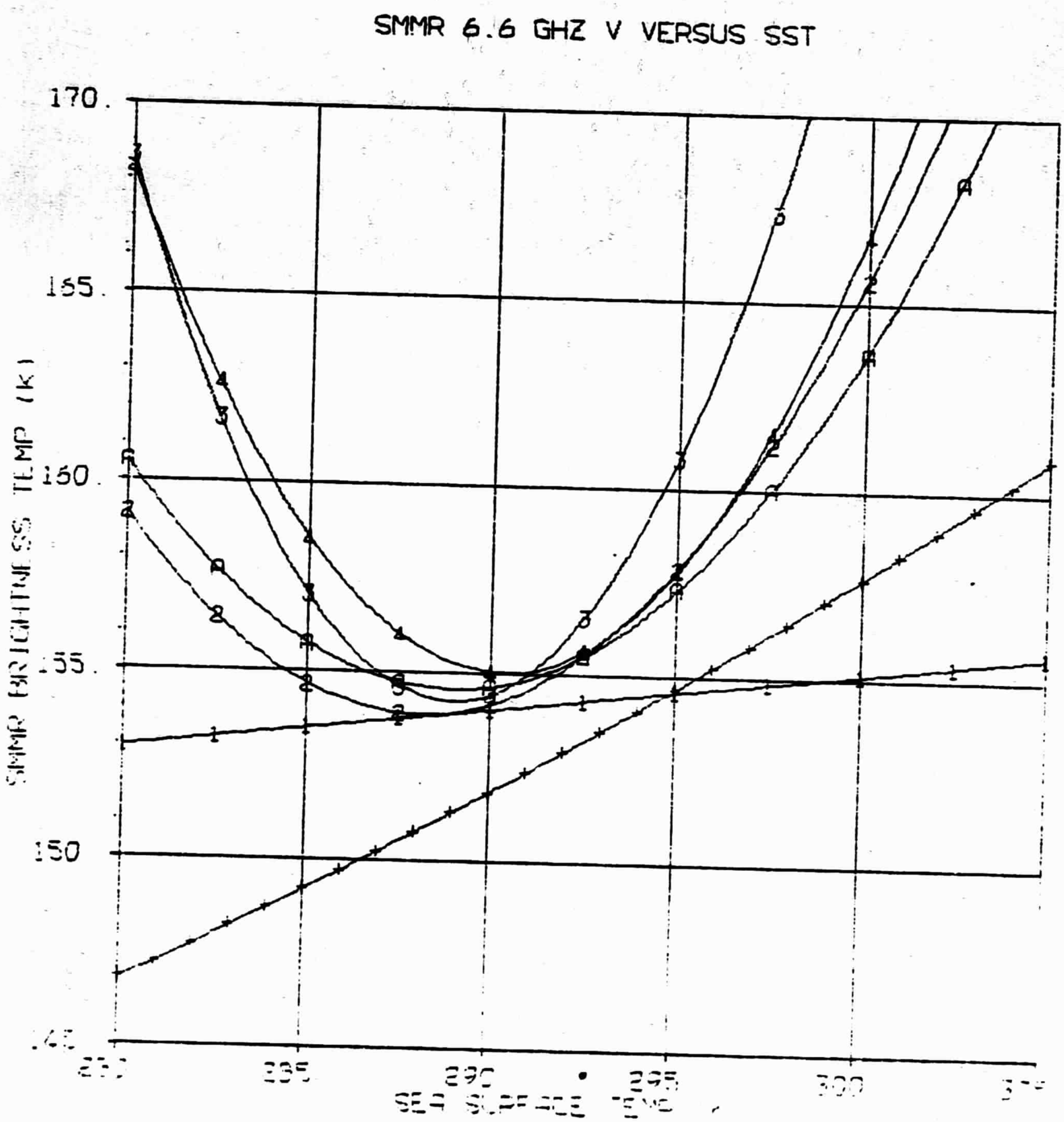

Figure 6.3

RUN 6

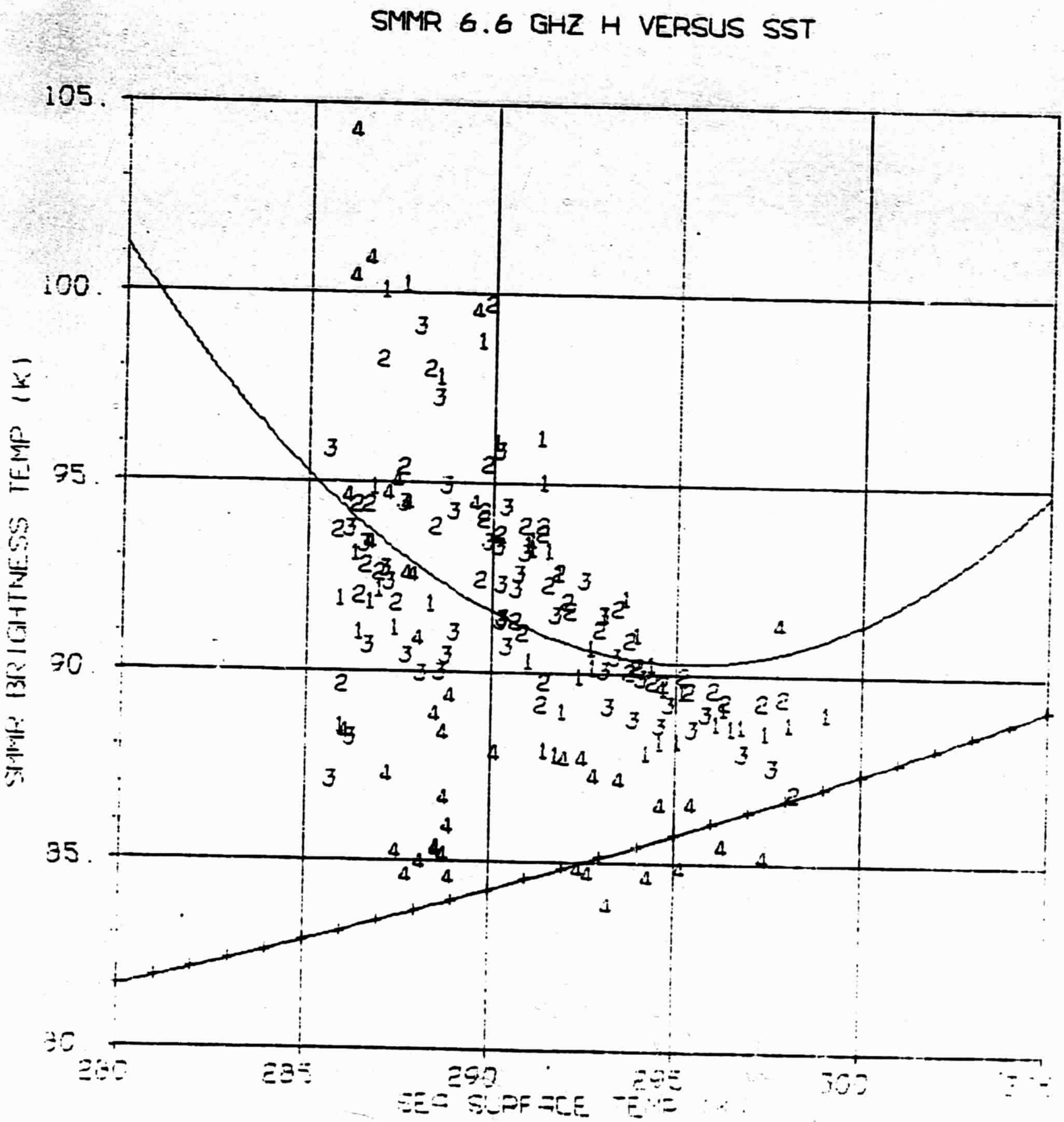

Figure 6.4

RUN 6 Curve Fits for

ORIGINAL PAGE IS OF POOR QUALITY

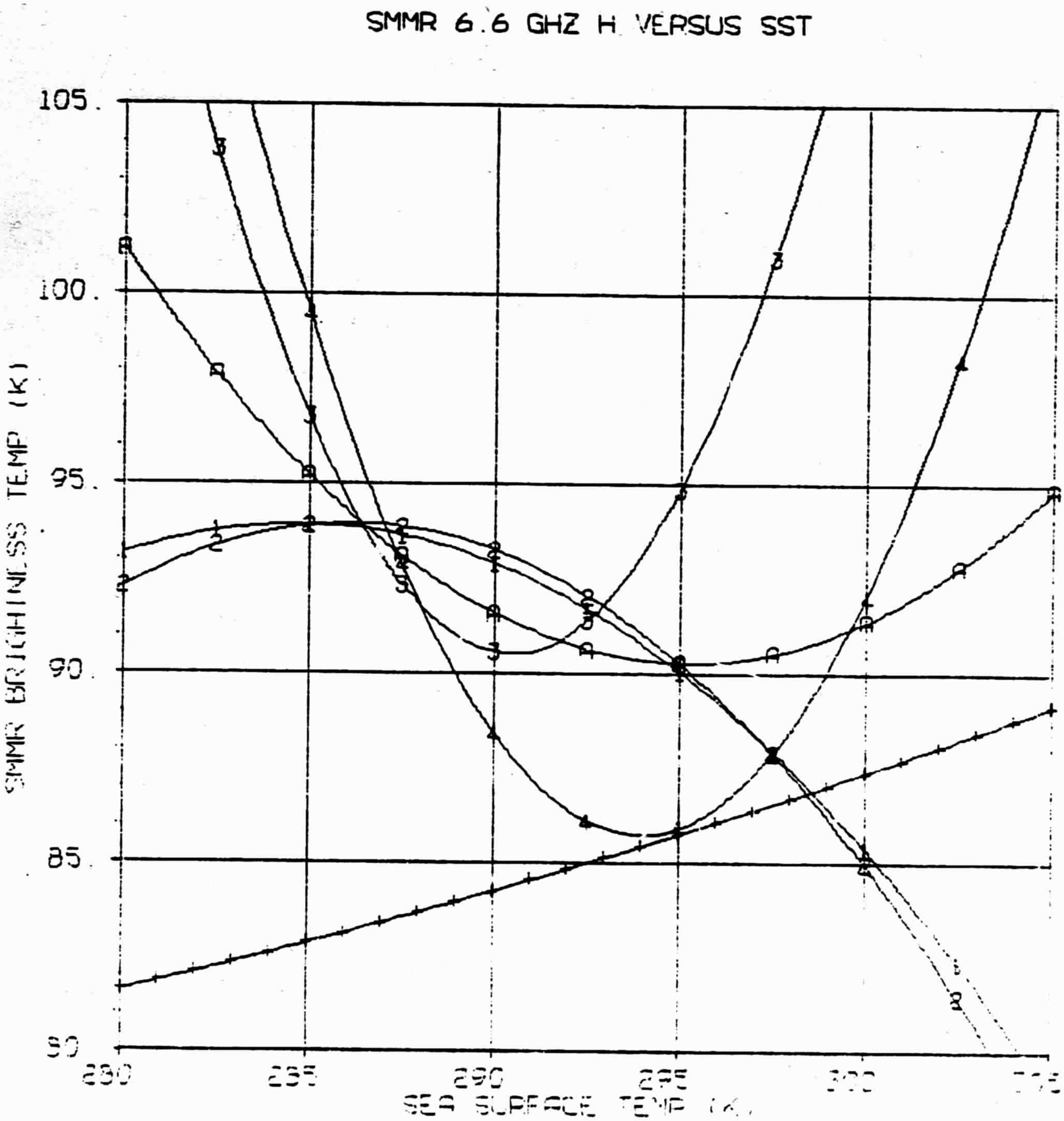

Table 7.

RUN 7 Statistical Summary

CURVE FITS FOR SMMR 6.6 GHZ VERSUS SST

COLUMN		CONSTANT TERM	LINEAR TERM	QUADRATIC TERM	RMS
1	V	201.28	-.16	.0000	.610
2	V	5246.07	-34.95	.0599	.555
3	V	14699.06	-99.58	.1704	.417
4	V	8605.64	-57.98	.0994	.635
ALL	V	7338.93	-49.18	.0842	.748
1	H	5038.29	-33.62	.0571	.525
2	H	7075.74	-47.75	.0816	.560
3	H	12861.74	-87.46	.1497	.638
4	H	13114.27	-89.15	.1525	.765
ALL	H	11792.28	-79.90	.1364	1.917

DISPERSION ABOUT STANDARD ATMOSPHERE - LOW WIND SPEED CURVE

COLUMN		BIAS	RMS
1	V	-1.12	1.566
2	V	-.96	.761
3	V	-1.00	.533
4	V	-.79	.737
ALL	V	-.97	.989
1	H	4.05	1.007
2	H	3.20	.624
3	H	1.59	.735
4	H	-.64	.902
ALL	H	2.05	1.970

Figure 7.1

RUN 7

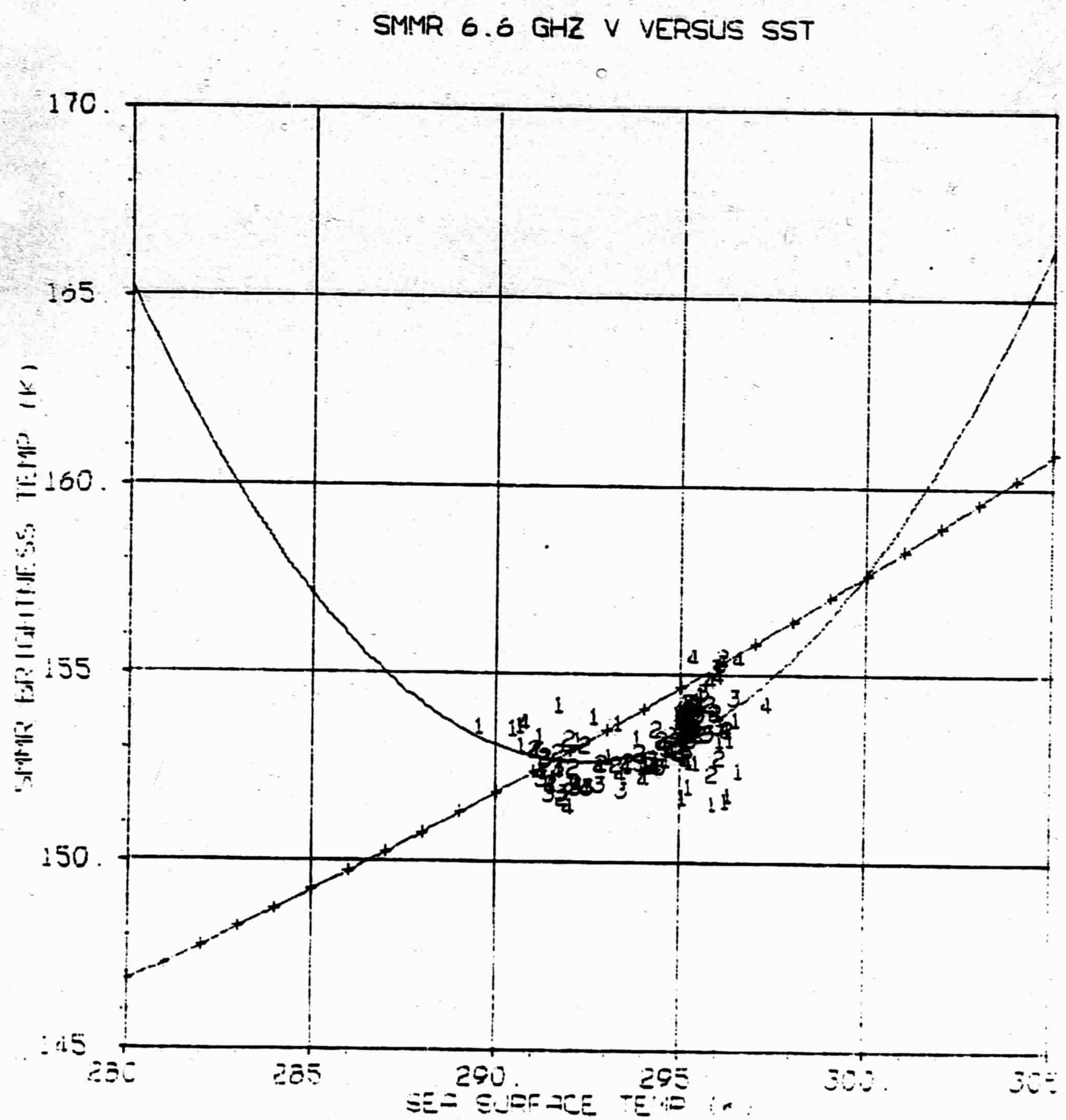

Figure 7.2

RUN 7 Curve Fits for

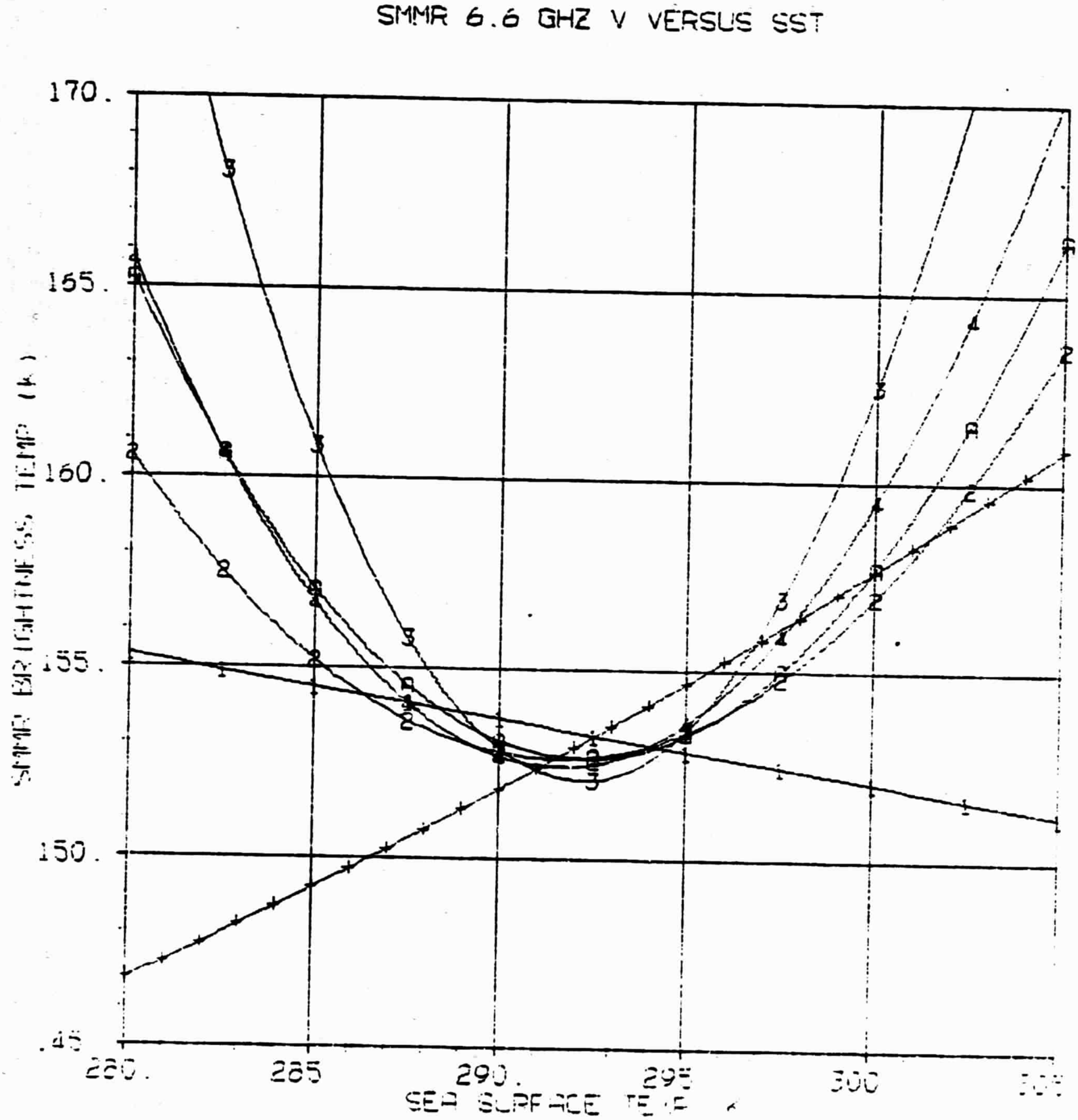

Figure 7.3

RUN 7

ORIGINAL PAGE IS OF POOR QUALITY

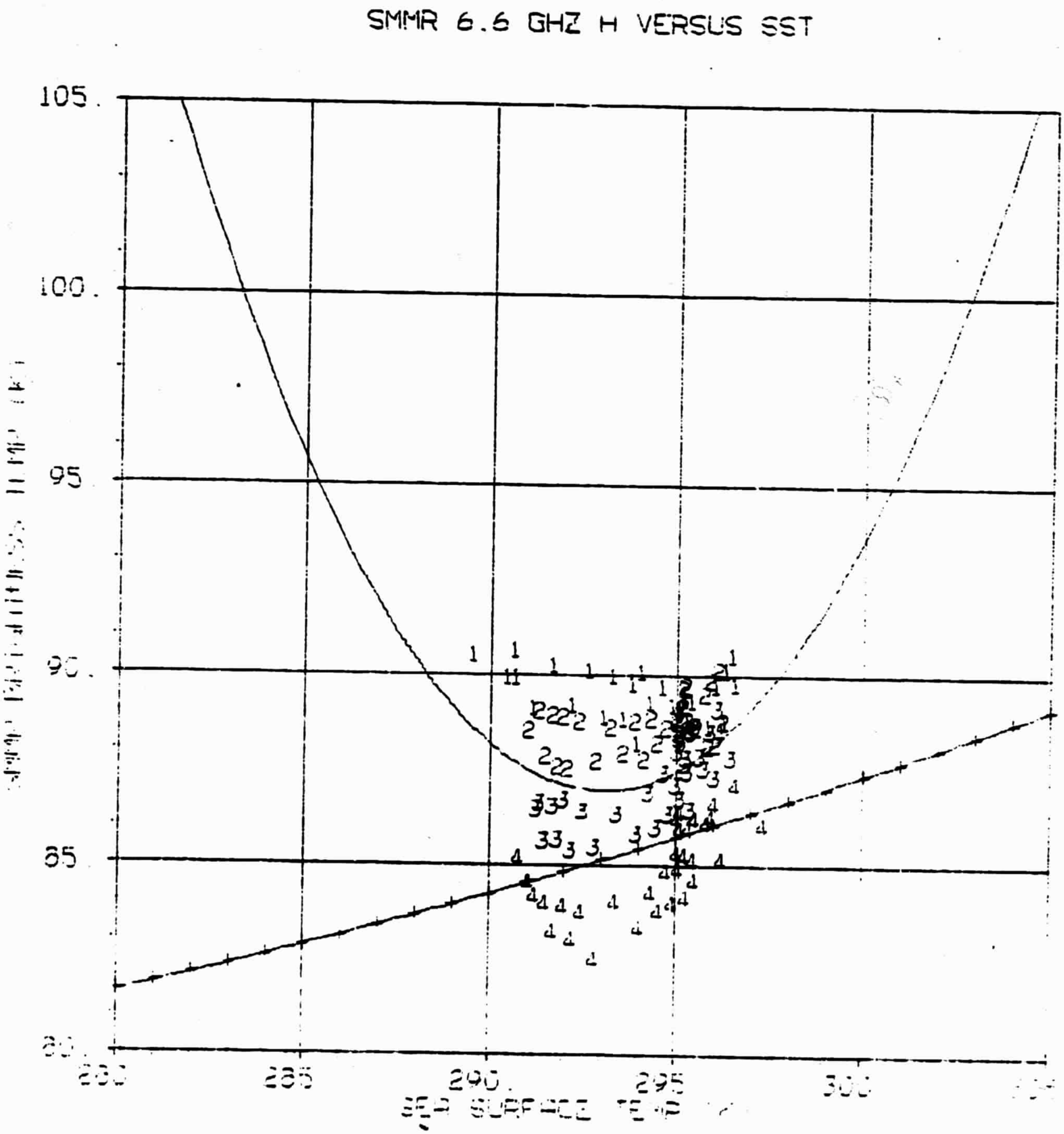

Figure 7.4

RUN 7 Curve Fits for

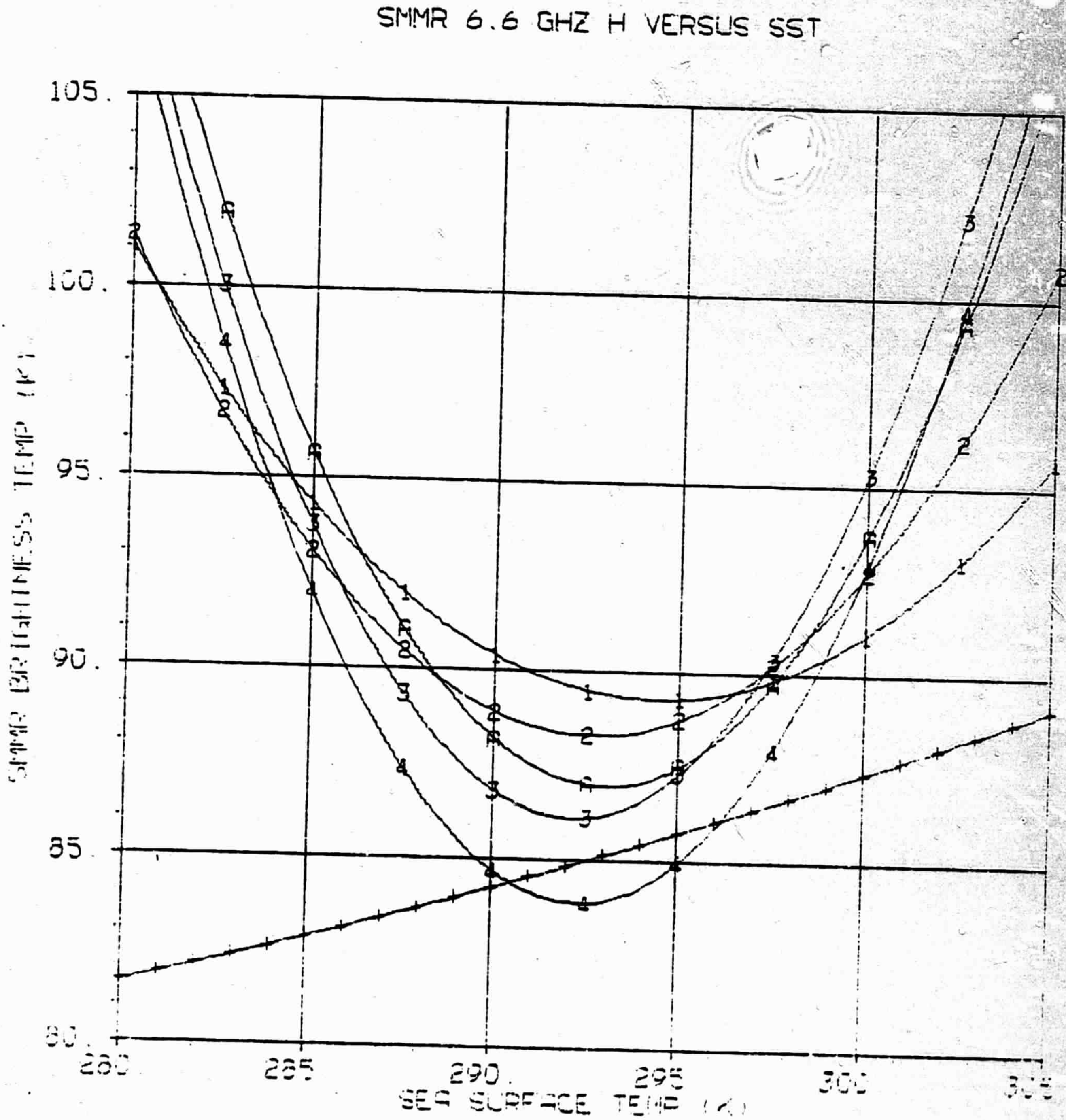

Table 8.

RUN 8 Statistical Summary

CURVE FITS FOR SMMR 6.6 GHZ VERSUS SST

COLUMN		CONSTANT TERM	LINEAR TERM	QUADRATIC TERM	RMS
1	V	787.82	-4.84	.0091	.748
2	V	1118.49	-7.07	.0129	.817
3	V	1623.81	-10.52	.0188	.873
4	V	3235.43	-21.52	.0375	1.062
ALL	V	2062.30	-13.52	.0239	1.088
1	H	4693.87	-31.68	.0545	1.541
2	H	3571.40	-23.98	.0412	1.518
3	H	2939.45	-19.57	.0336	1.692
4	H	5327.82	-35.83	.0612	1.830
ALL	H	3964.51	-26.61	.0456	2.040

DISPERSION ABOUT STANDARD ATMOSPHERE - LOW WIND SPEED CURVE

COLUMN		BIAS	RMS
1	V	-2.75	.858
2	V	-1.90	1.048
3	V	-1.54	1.191
4	V	-1.00	1.639
ALL	V	-1.80	1.376
1	H	3.13	1.909
2	H	2.68	1.975
3	H	1.83	2.396
4	H	.62	3.229
ALL	H	2.06	2.616

Figure 8.1

RUN 8

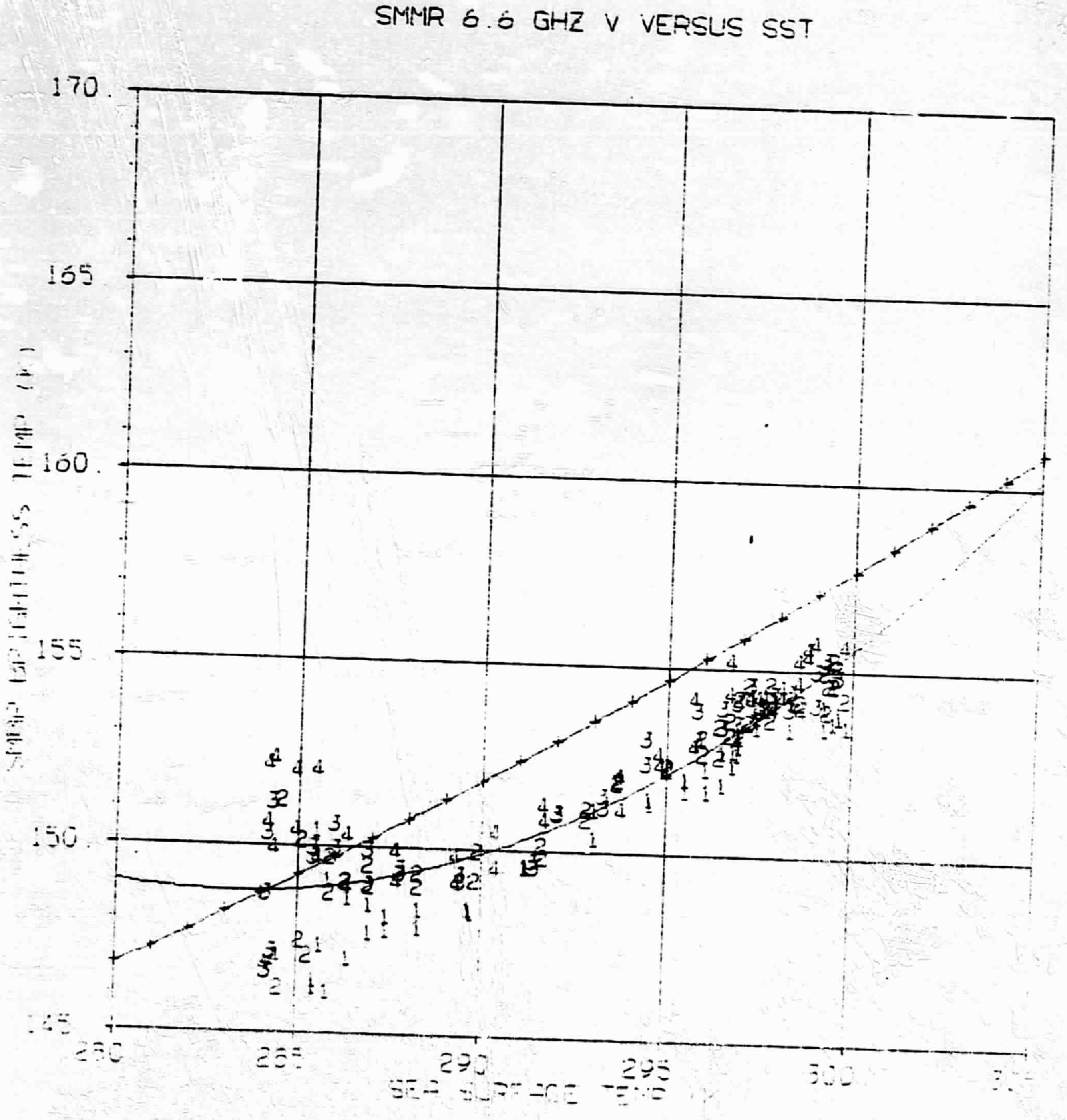

Figure 8.2

RUN 8 Curve Fits for

ORIGINAL PAGE IS
OF POOR QUALITY

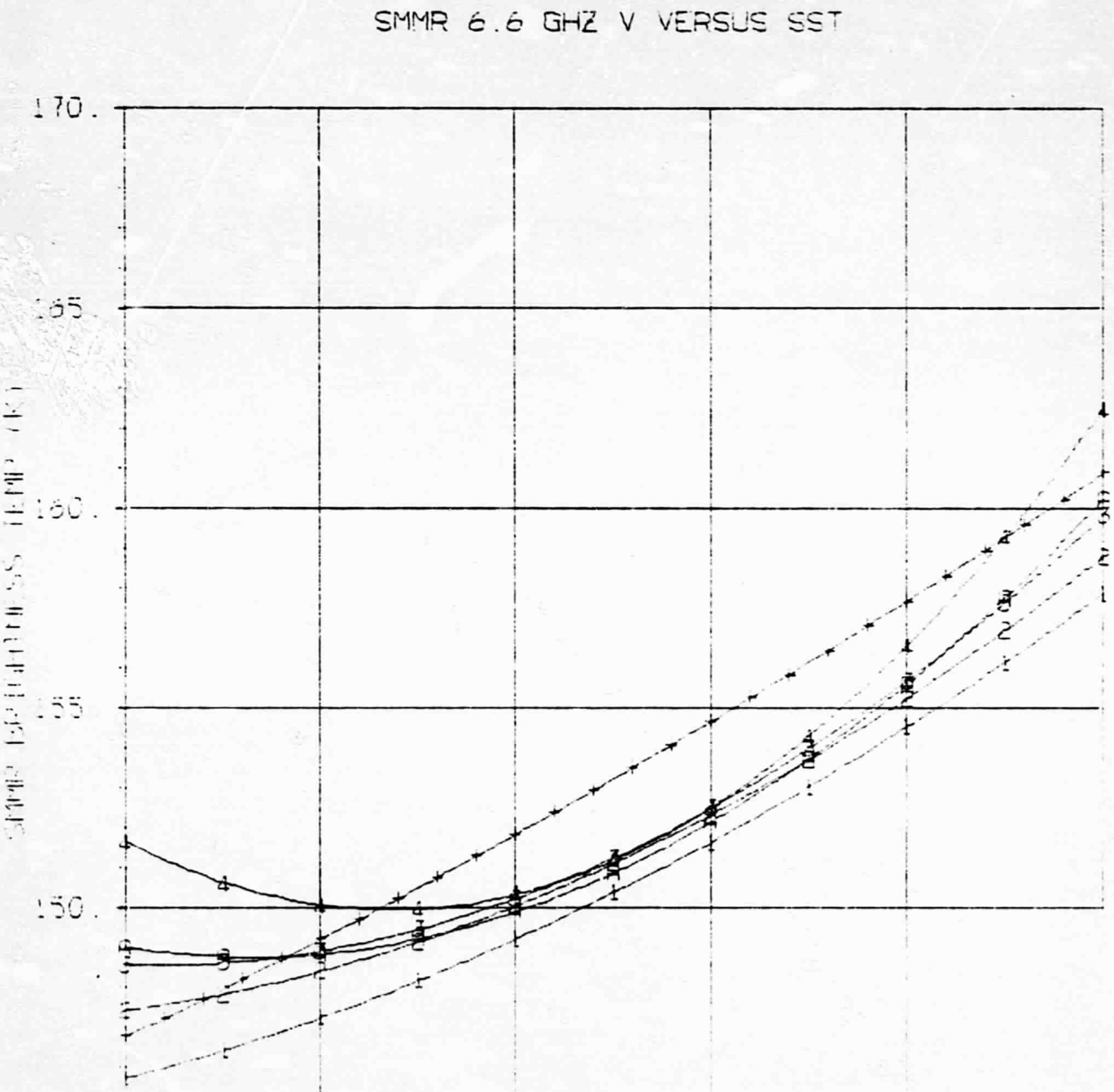

Figure 8.3

RUN 8

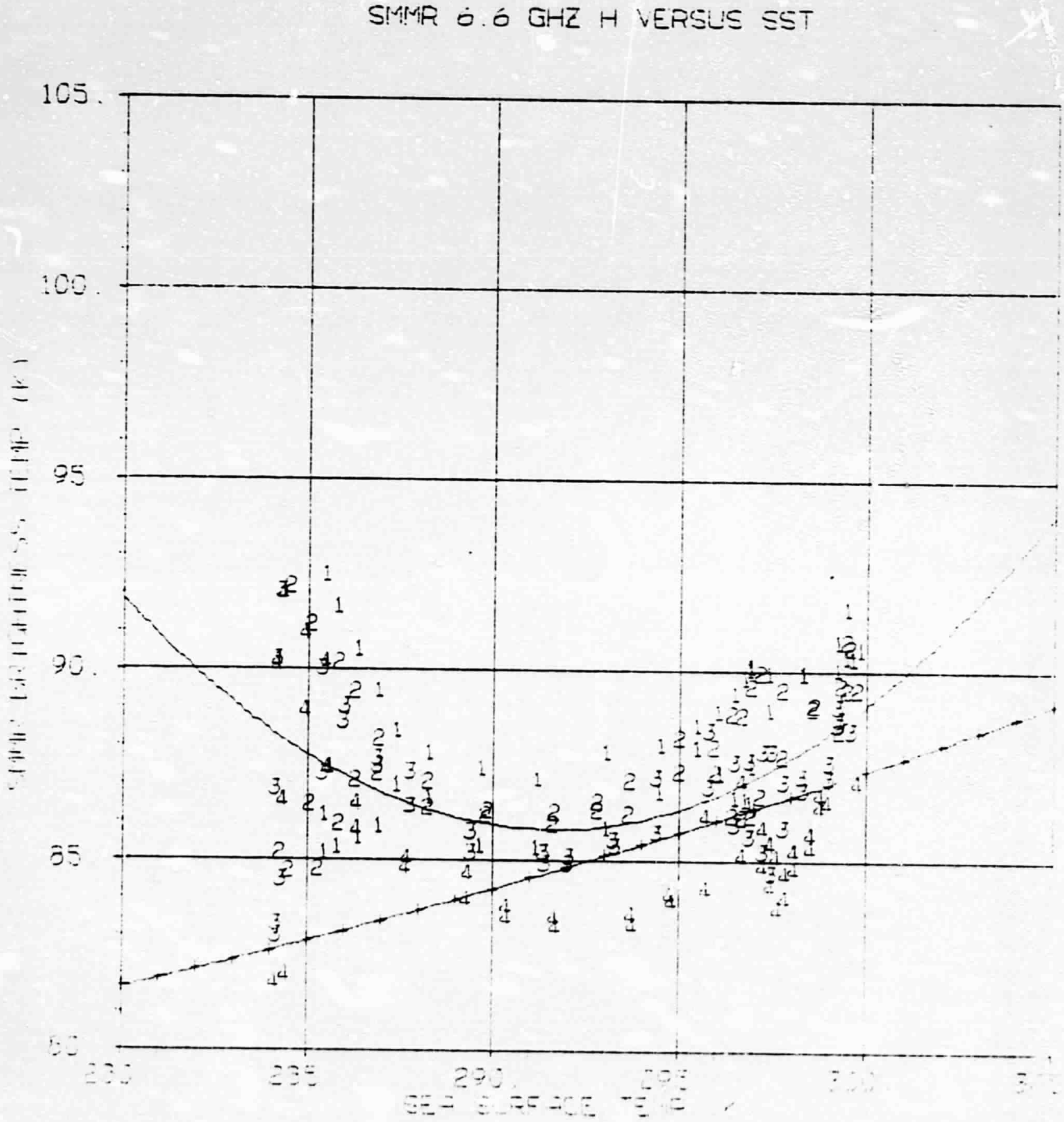

Figure 8.4

RUN 8 Curve Fits for

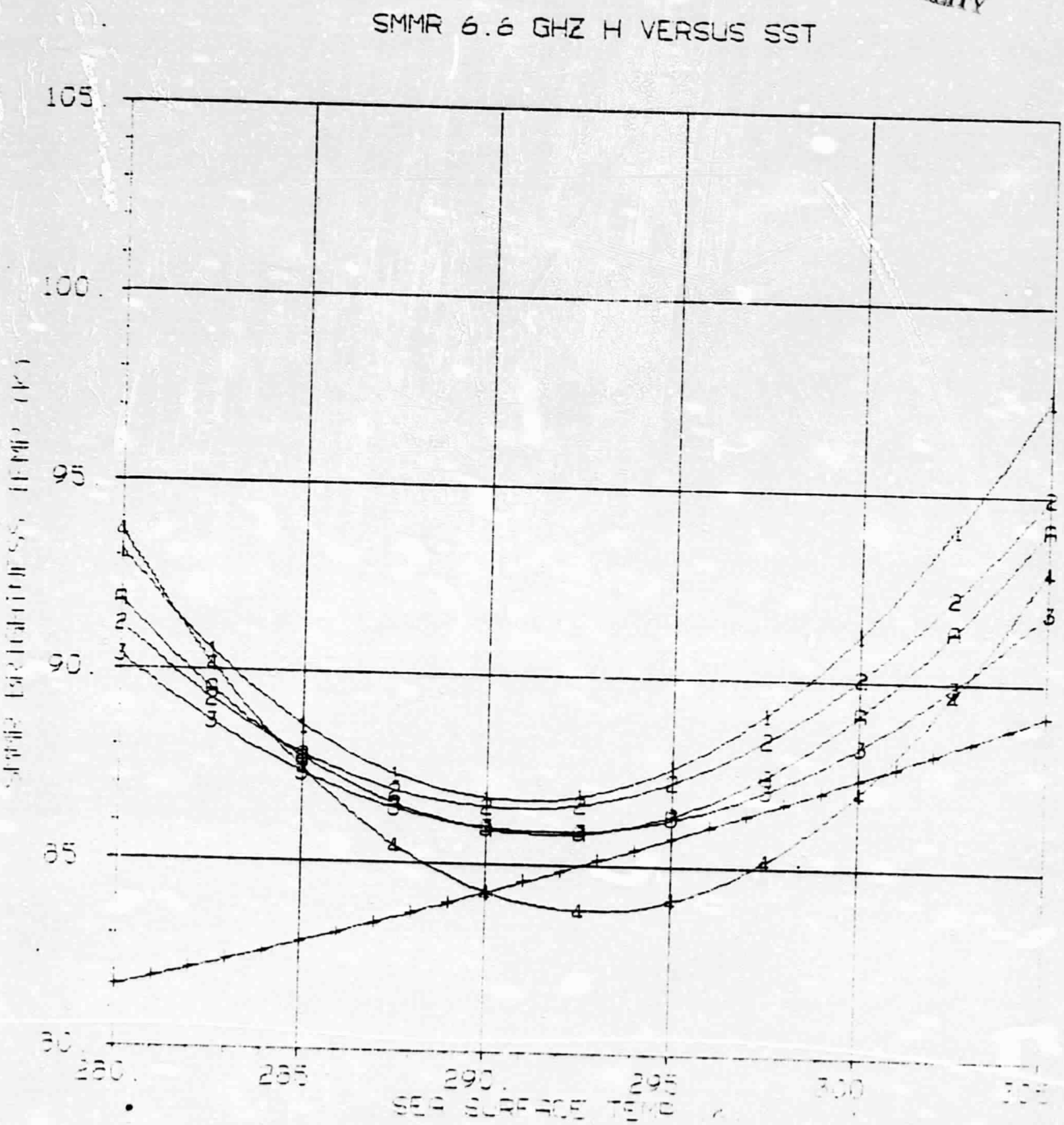

Table 9.

RUN 9 Statistical Summary

CURVE FITS FOR SMMR 6.6 GHZ VERSUS SST

COLUMN	CONSTANT TERM	LINEAR TERM	QUADRATIC TERM	RMS
1 V	-1624.73	11.78	-.0195	2.035
2 V	-1055.49	7.89	-.0128	2.539
3 V	-965.83	7.31	-.0119	3.437
4 V	-905.89	6.98	-.0115	2.512
ALL V	-904.97	6.90	-.0112	2.763
1 H	61.86	.09	.0000	2.769
2 H	88.97	.00	.0000	2.582
3 H	88.20	.00	.0000	4.315
4 H	142.67	-.19	.0000	3.797
ALL H	88.25	.00	.0000	3.632

DISPERSION ABOUT STANDARD ATMOSPHERE - LOW WIND SPEED CURVE

COLUMN	BIAS	RMS
1 V	-1.64	2.211
2 V	-.74	2.671
3 V	-.27	3.576
4 V	.17	2.861
ALL V	-.62	2.950
1 H	4.07	2.907
2 H	3.80	2.868
3 H	3.09	4.560
4 H	1.54	4.456
ALL H	3.13	3.9[illegible]1

Figure 9.1

RUN 9

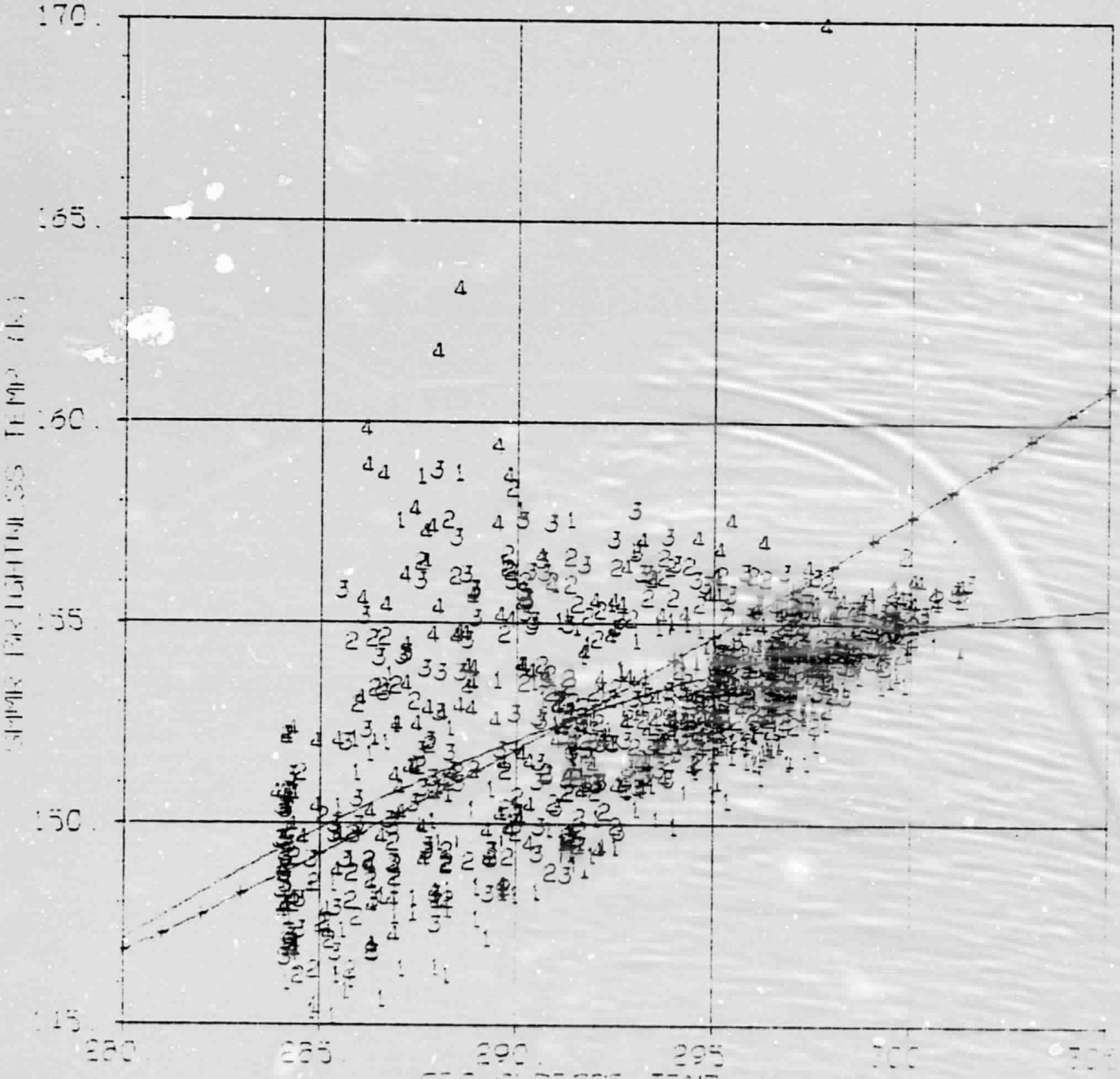

Figure 9.2

RUN 9 Curve Fits for

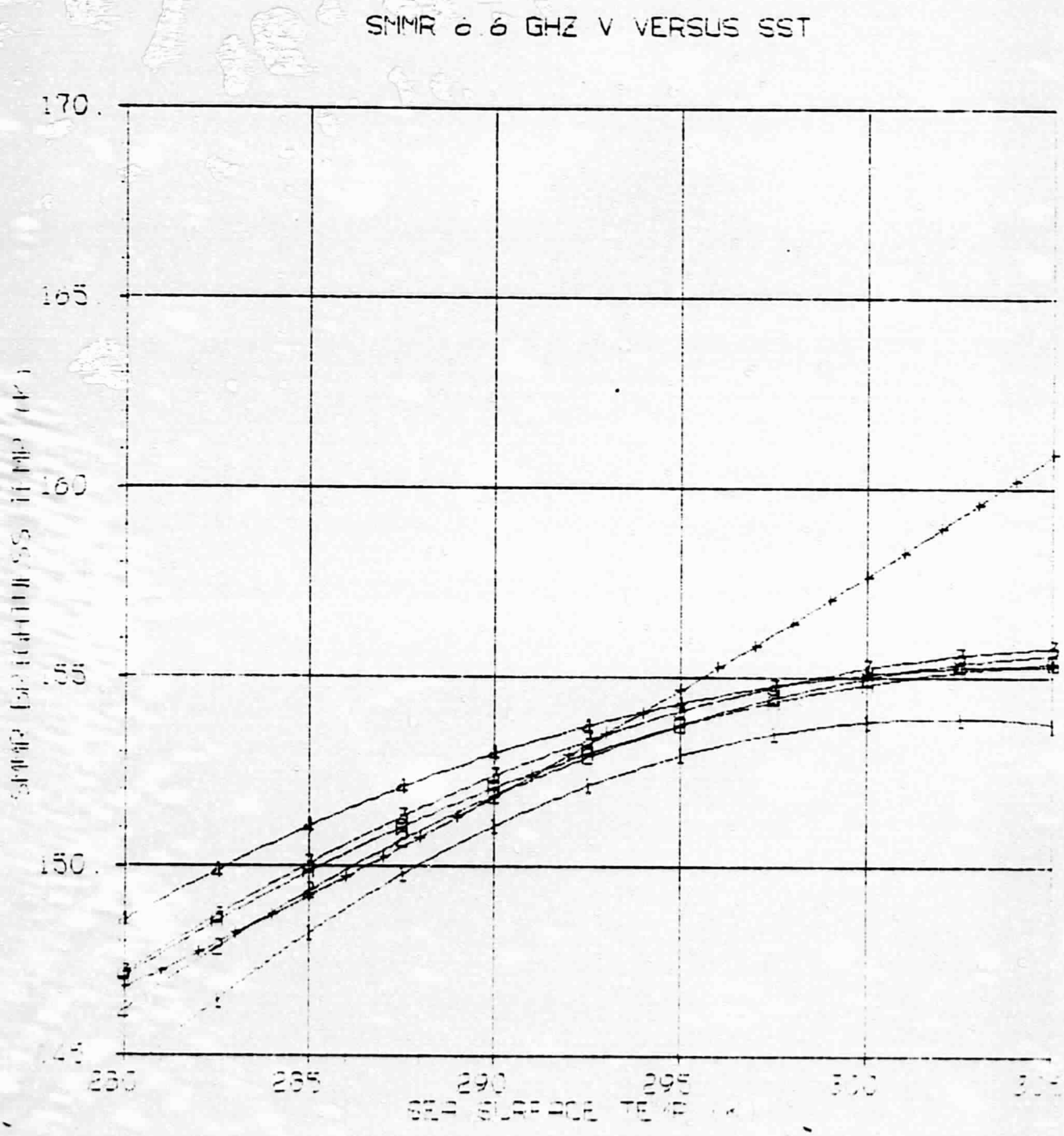

Figure 9.3

RUN 9

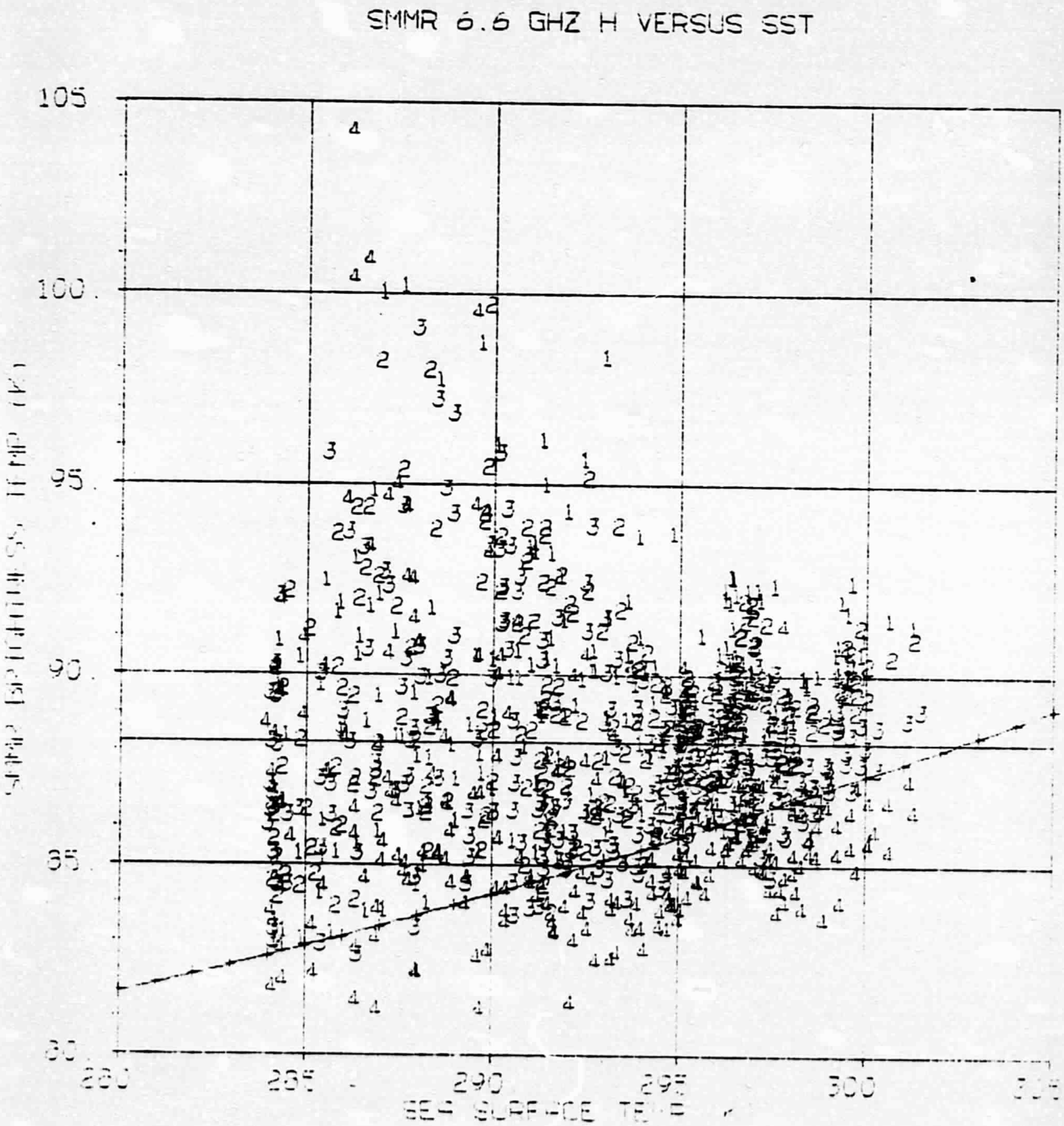

Figure 9.4

RUN 9 Curve Fits for

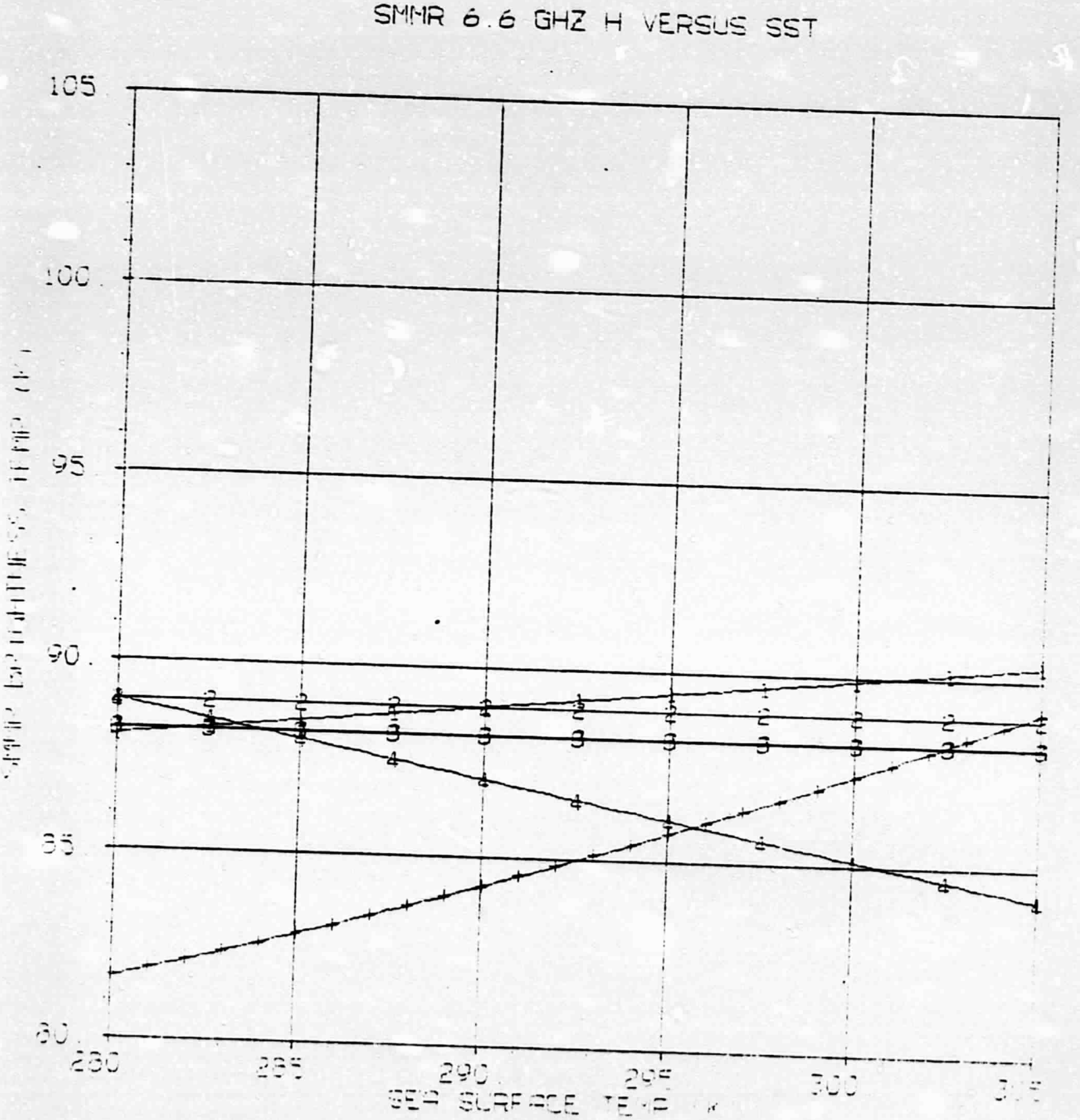

Table 10.

RUN 10 Statistical Summary

CURVE FITS FOR SMMR 6.6 GHZ VERSUS SST

COLUMN		CONSTANT TERM	LINEAR TERM	QUADRATIC TERM	RMS
1	V	-897.09	6.69	-.0106	1.374
2	V	21.75	.44	.0000	1.141
3	V	31.63	.41	.0000	1.148
4	V	40.31	.38	.0000	1.444
ALL	V	27.92	.42	.0000	1.405
1	H	19.79	.24	.0000	2.156
2	H	42.57	.16	.0000	1.833
3	H	962.56	-6.05	.0104	1.945
4	H	1339.91	-8.56	.0146	2.303
ALL	H	592.98	-3.57	.0063	2.410

DISPERSION ABOUT STANDARD ATMOSPHERE - LOW WIND SPEED CURVE

COLUMN		BIAS	RMS
1	V	-2.31	1.442
2	V	-1.58	1.261
3	V	-1.31	1.346
4	V	-.78	1.683
ALL	V	-1.50	1.544
1	H	3.45	2.173
2	H	2.98	1.942
3	H	1.94	2.276
4	H	.55	2.819
ALL	H	2.23	2.577

Figure 10.1

RUN 10

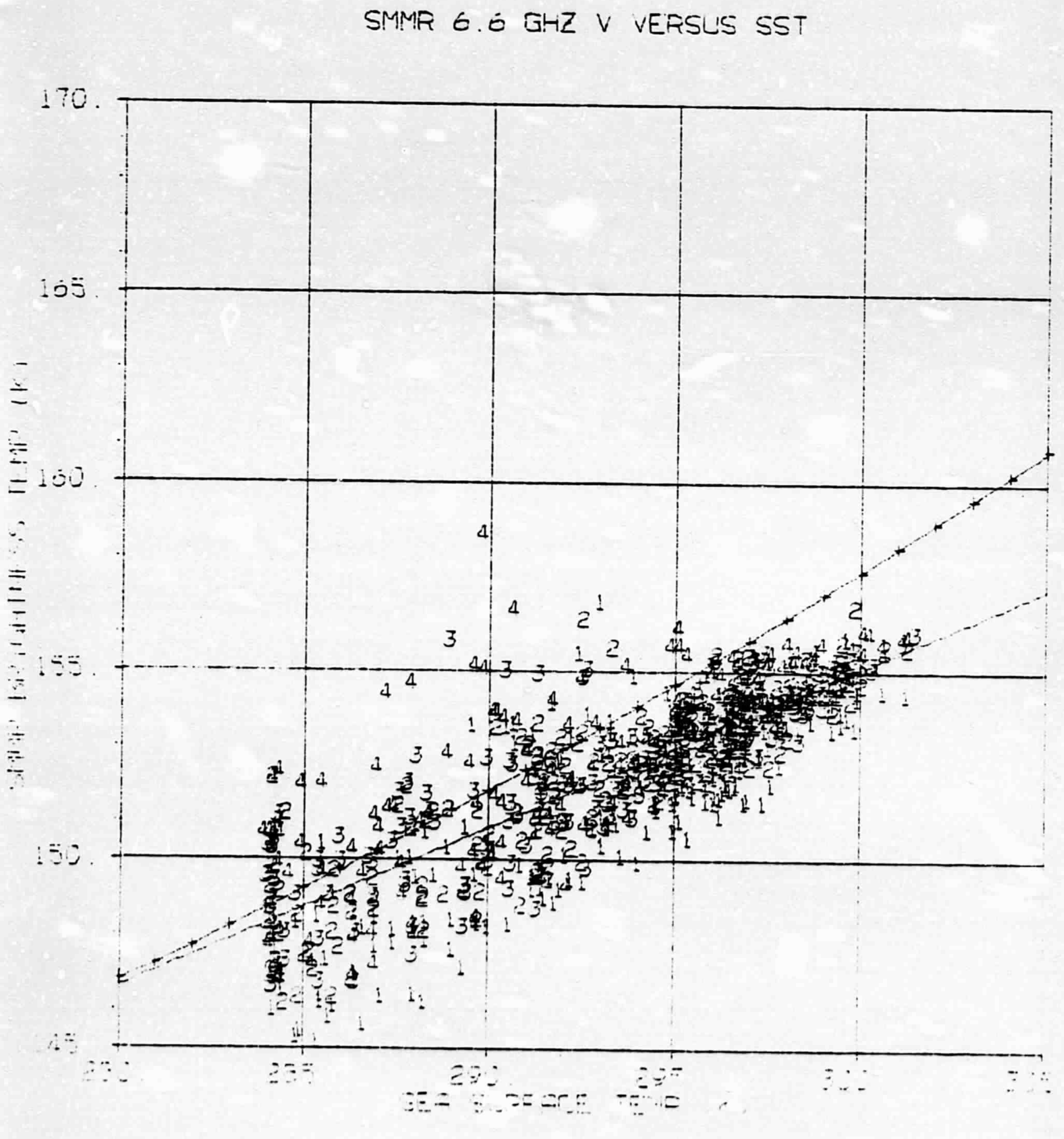

Figure 10.2

RUN 10 Curve Fits for

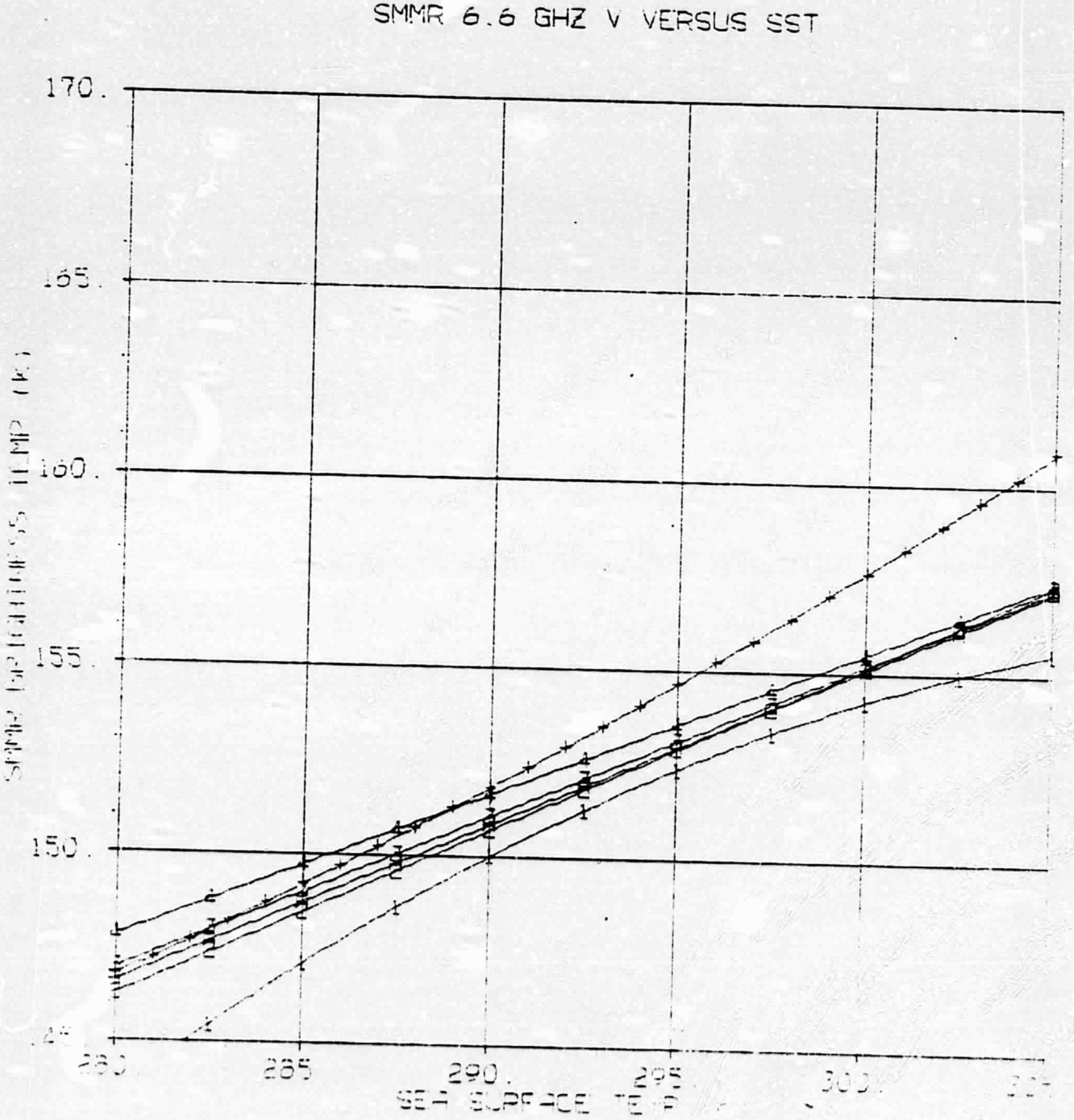

Figure 10.3

RUN 10

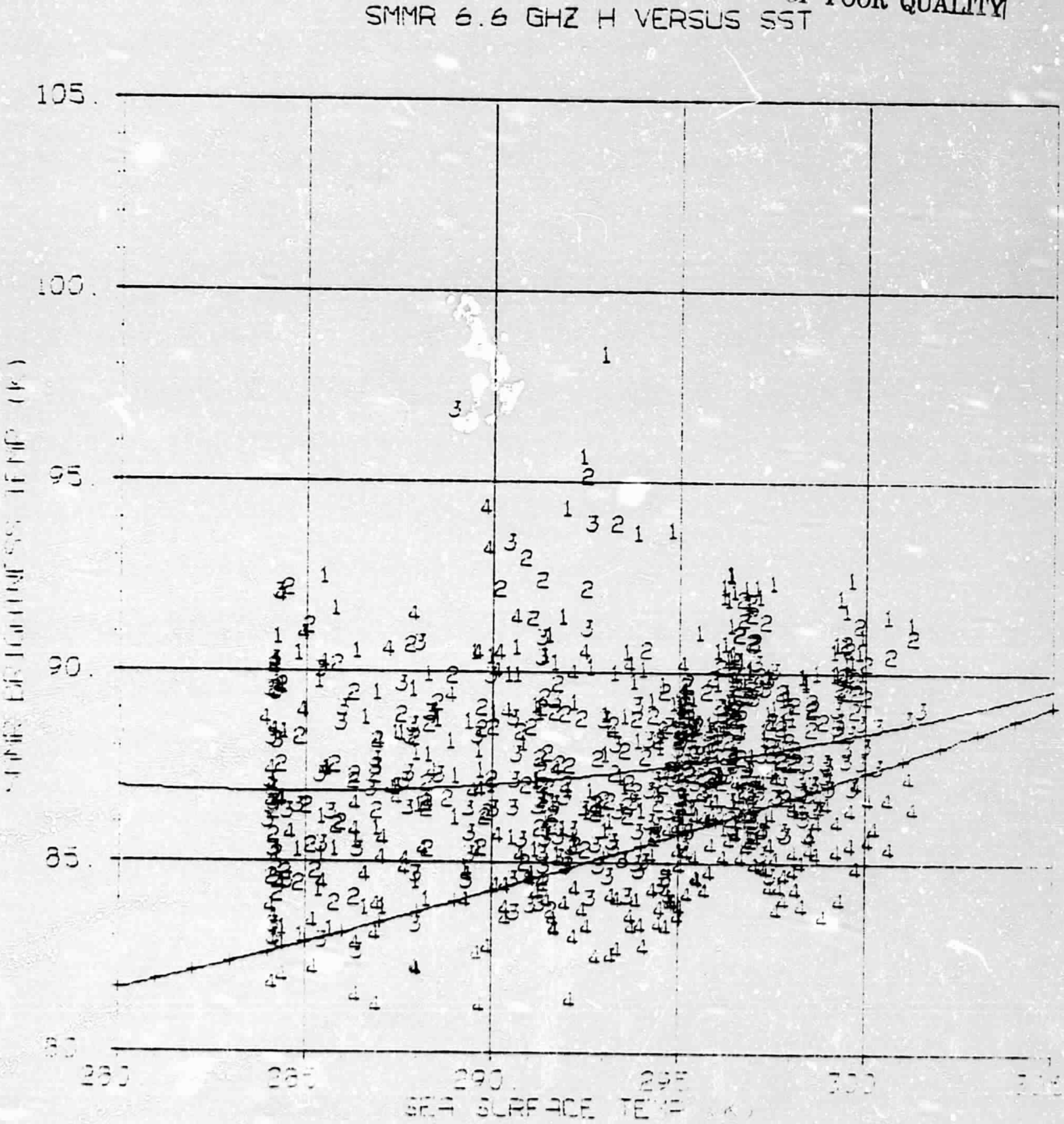

Figure 10.4

RUN 10 Curve Fits for

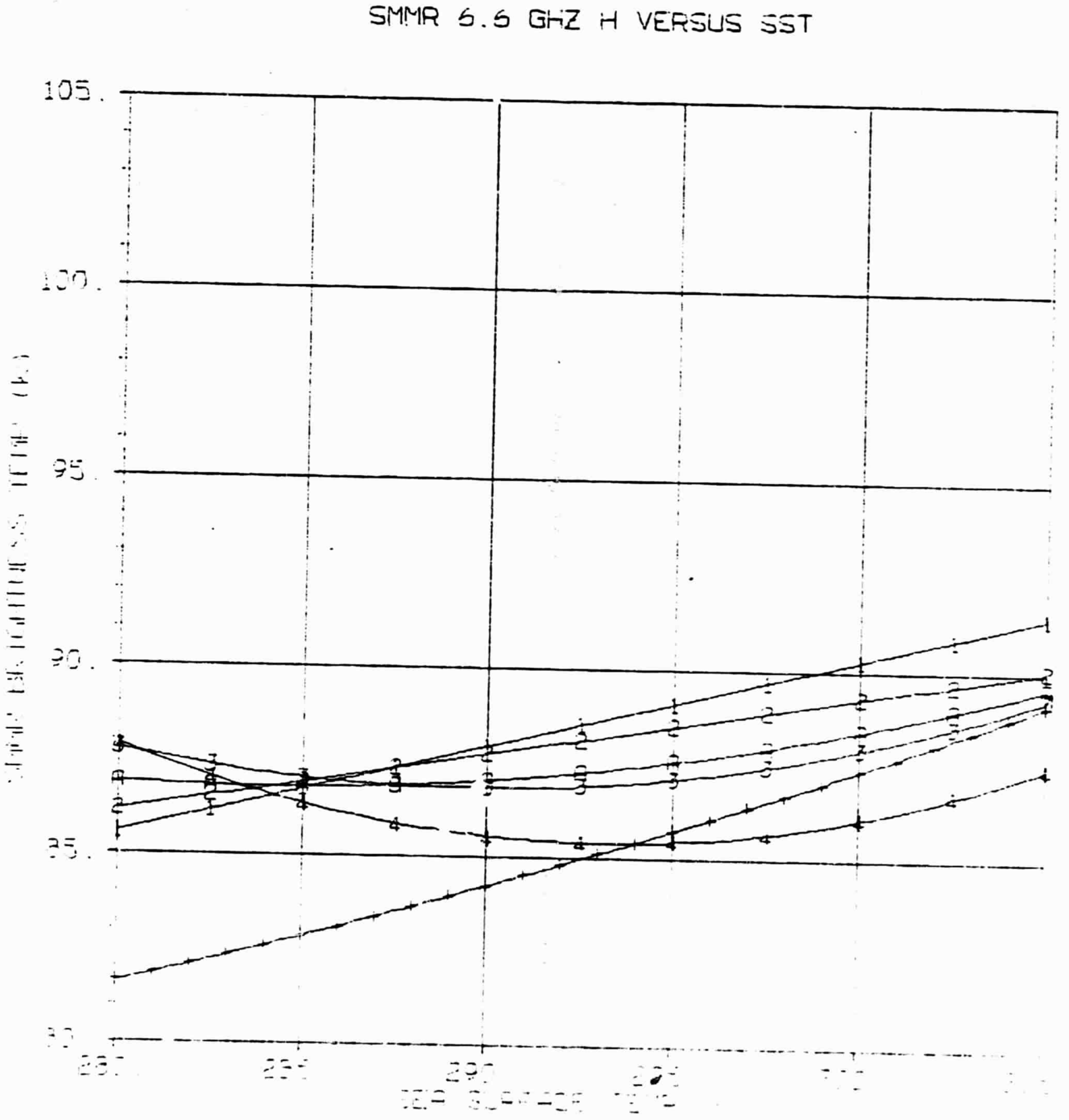

Table 11.1

RUN 11-1

CURVE FITS FOR SMMR 6.6 GHZ TB VERSUS CELL NUMBER

			V POL.			H POL.		
BLOCK	ROW	AVERAGE LATITUDE	LINEAR TERM	CONSTANT TERM	RMS	LINEAR TERM	CONSTANT TERM	RMS
1	1	50.84	.568	149.895	.260	-.162	92.605	.061
	2	49.63	.470	148.900	.212	-.566	92.240	.145
	3	48.42	.569	148.265	.194	-.487	91.170	.224
	4	47.20	.460	148.165	.258	-.652	90.485	.404
2	1	45.98	.242	148.170	.212	-.824	89.600	.420
	2	44.75	.234	148.455	.312	-.803	88.835	.533
	3	43.51	.000	149.132	.587	-.887	88.275	.134
	4	42.27	.000	149.640	.120	-1.138	88.395	.102
3	1	41.03	.144	150.425	.155	-1.520	89.510	.132
	2	39.79	.000	151.420	.319	-1.598	89.980	.278
	3	38.54	.000	152.475	.378	-1.320	90.160	.881
	4	37.29	.859	150.980	.200	.000	87.322	.799
4	1	36.03	1.063	150.610	.290	.000	86.500	.443
	2	34.78	.563	151.955	.098	-.584	87.290	.068
	3	33.52	.420	152.360	.027	-.758	87.485	.144
	4	32.26	.323	152.825	.200	-1.331	89.015	.262
5	1	31.00	.199	153.335	.136	-1.671	90.855	.159
	2	29.73	.000	154.232	.154	-1.778	92.145	.355
	3	28.46	.216	154.065	.231	-1.832	92.930	.275
	4	27.20	.235	154.585	.174	-1.772	93.860	.368

Figure 11.1

RUN 11-1

SMMR 6.6 GHZ TB CROSS-TRACK GRADIENT VERSUS LATITUDE

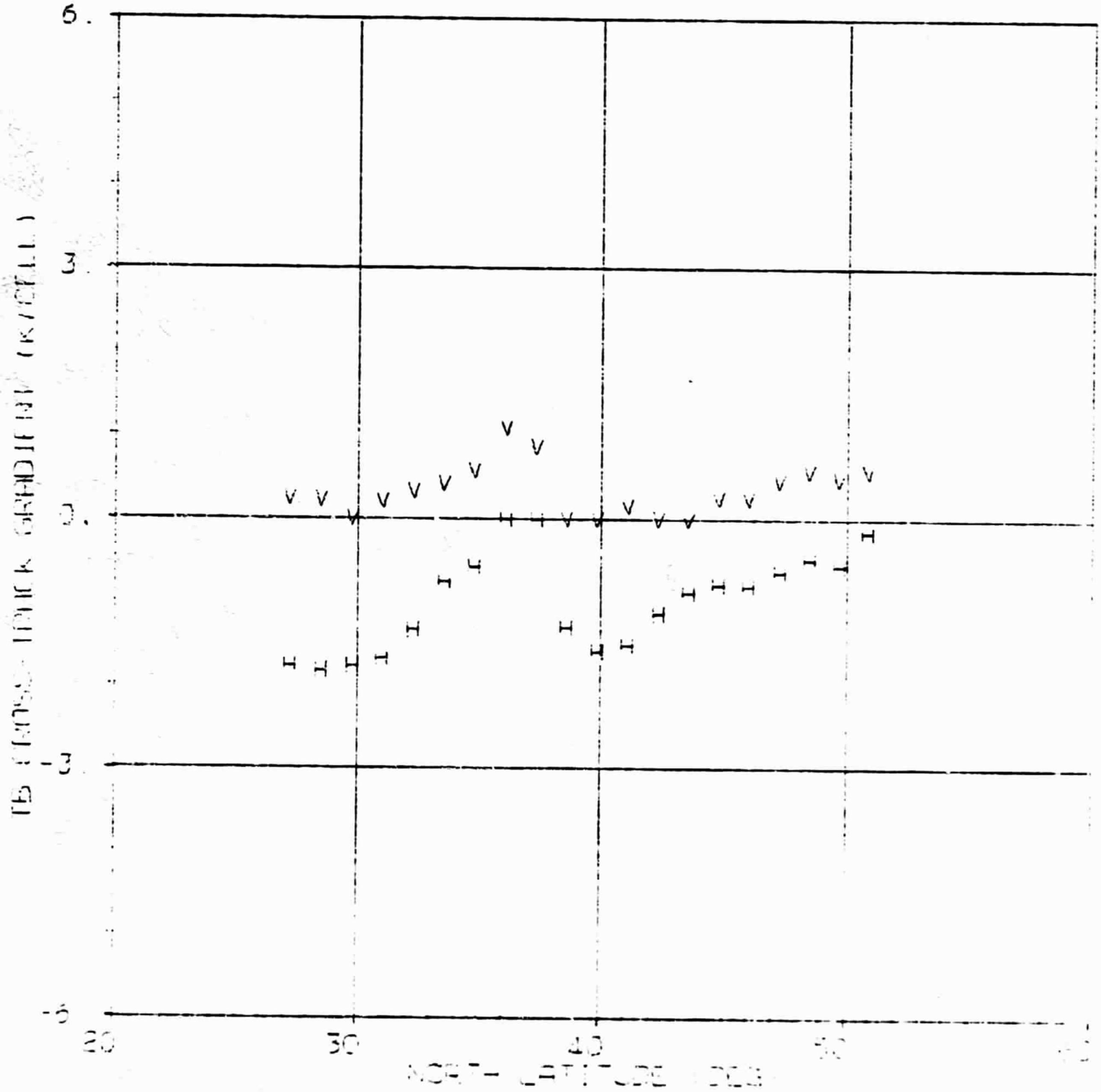

Table 12.1

RUN 12-1

CURVE FITS FOR SMMR 6.6 GHZ TB VERSUS CELL NUMBER

BLOCK	ROW	AVERAGE LATITUDE	V POL. LINEAR TERM	V POL. CONSTANT TERM	V POL. RMS	H POL. LINEAR TERM	H POL. CONSTANT TERM	H POL. RMS
1	1	47.77	1.201	149.075	.533	.000	89.375	.935
	2	46.55	1.200	149.180	.685	.885	87.205	.726
	3	45.32	1.634	147.940	.621	1.523	85.740	1.306
	4	44.09	1.282	148.405	.437	.933	85.595	.745
2	1	42.86	.858	149.015	.434	.000	86.655	.336
	2	41.61	.664	149.255	.353	-.386	87.180	.385
	3	40.37	.616	149.480	.202	-.874	88.155	.422
	4	39.12	.301	150.900	.311	-.957	88.110	.313
3	1	37.87	.582	150.540	.290	-.754	87.345	.424
	2	36.62	.565	150.565	.284	-.626	86.635	.200
	3	35.37	.489	150.645	.053	-1.124	87.925	.224
	4	34.11	.230	151.695	.096	-1.451	89.635	.224
4	1	32.85	.204	152.545	.103	-1.525	90.965	.304
	2	31.59	.225	153.010	.073	-1.456	91.610	.272
	3	30.32	.285	153.395	.278	-1.525	92.690	.258
	4	29.06	.138	154.370	.140	-1.393	93.560	.189
5	1	27.79	.449	153.935	.406	-1.756	95.010	.763
	2	26.53	.392	153.910	.295	-1.609	94.475	.628
	3	25.26	.525	153.380	.253	-1.546	93.935	.186
	4	23.99	.398	153.855	.136	-1.471	94.125	.290

Figure 12.1

RUN 12-1

SMMR 6.6 GHZ TB CROSS-TRACK GRADIENT VERSUS LATITUDE

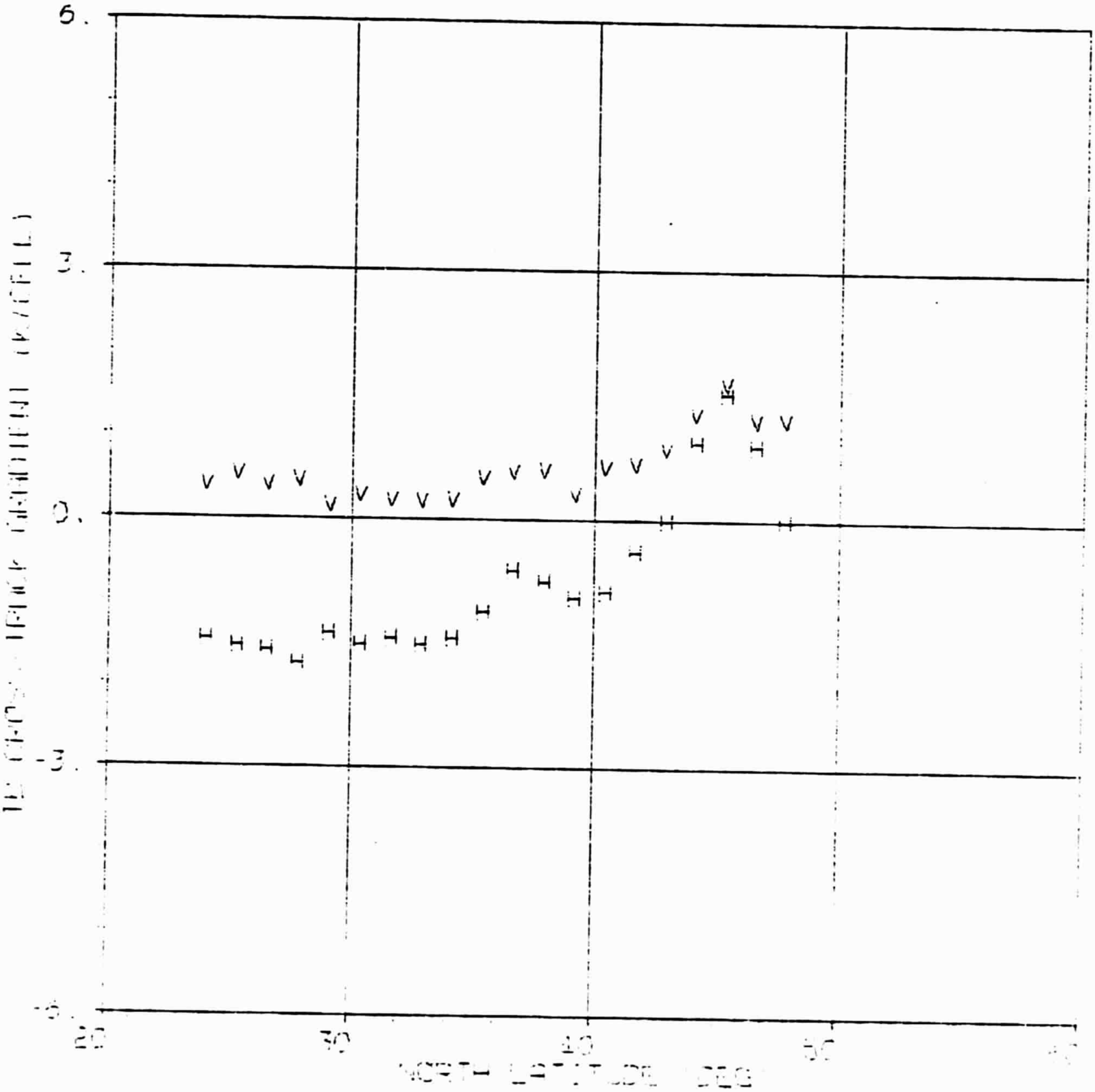

Table 13.1

RUN 13-1

CURVE FITS FOR SMMR 6.6 GHZ TB VERSUS CELL NUMBER

			V POL.			H POL.		
BLOCK	ROW	AVERA E LATITUDE	LINEAR TERM	CONSTANT TERM	RMS	LINEAR TERM	CONSTANT TERM	RMS
1	1	53.47	1.301	145.535	.083	.000	88.225	.442
	2	52.28	1.135	146.765	.253	-.062	89.750	.083
	3	51.08	.000	150.950	.753	-.802	91.775	.100
	4	49.87	.000	149.172	.575	-1.301	91.970	.183
2	1	48.66	-.161	148.710	.093	-1.789	91.675	.125
	2	47.45	-.127	148.320	.025	-1.815	90.855	.221
	3	46.22	.000	148.202	.237	-1.699	90.090	.487
	4	44.99	.000	148.455	.350	-1.441	89.025	.266
3	1	43.76	.000	148.310	.067	-1.530	88.625	.284
	2	42.52	-.239	149.410	.068	-1.506	87.785	.476
	3	41.28	-.250	150.445	.069	-1.811	89.000	.328
	4	40.04	-.244	151.910	.100	-1.938	90.590	.314
4	1	38.79	-.417	153.675	.181	-2.140	92.980	.229
	2	37.54	.000	153.730	.435	-1.187	92.085	.635
	3	36.29	.296	152.935	.411	-.426	89.155	.359
	4	35.03	.396	152.900	.257	-.805	89.410	.312
5	1	33.77	.282	153.445	.322	-1.268	90.390	.324
	2	32.51	.351	153.285	.149	-1.334	90.785	.202
	3	31.25	.181	153.975	.093	-1.188	91.000	.147
	4	29.99	.384	153.720	.127	-1.229	91.570	.312
6	1	28.72	.656	153.615	.288	-1.348	92.390	.297
	2	27.45	.389	154.130	.123	-1.460	92.800	.325
	3	26.19	.436	154.395	.275	-1.452	93.150	.163
	4	24.92	.504	154.265	.323	-1.655	93.595	.575

Figure 13.1

RUN 13-1

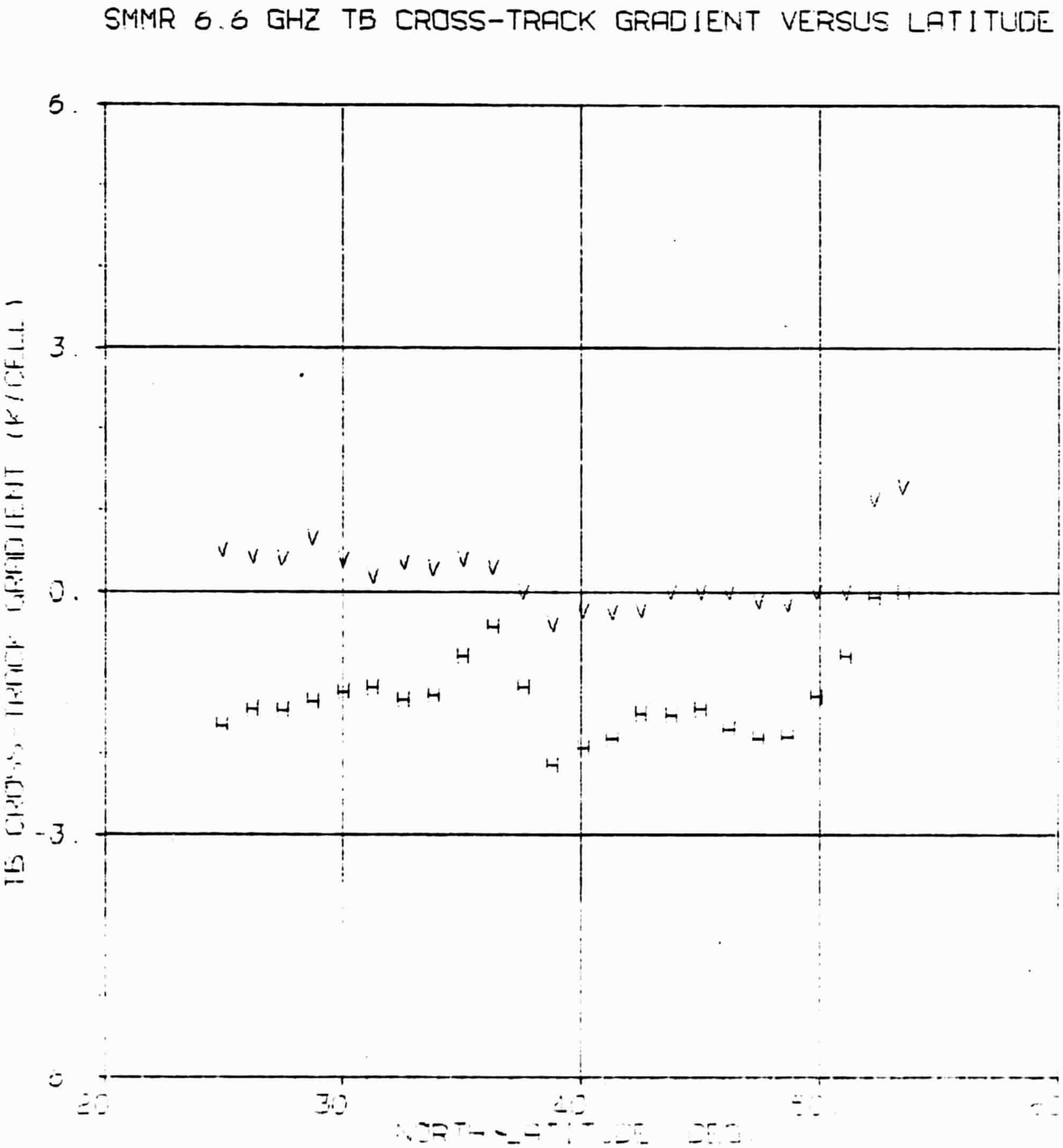

Table 14.1

RUN 14-1

CURVE FITS FOR SMMR 6.6 GHZ TB VERSUS CELL NUMBER

			V POL.			H POL.		
BLOCK	ROW	AVERAGE LATITUDE	LINEAR TERM	CONSTANT TERM	RMS	LINEAR TERM	CONSTANT TERM	RMS
1	1	25.16	.918	153.830	.285	-.657	90.015	.762
	2	26.42	.772	153.840	.185	-.809	90.625	.791
	3	27.69	.556	154.280	.361	-.705	90.875	.790
	4	28.96	.506	154.525	.148	-.685	91.110	.988
2	1	30.22	.000	156.147	1.045	.000	90.112	1.435
	2	31.49	.000	155.972	.751	.000	90.727	1.812
	3	32.75	.000	155.490	.588	-1.200	93.630	.910
	4	34.01	.433	154.450	.498	-.612	92.720	.847
3	1	35.26	1.341	152.625	.494	1.187	89.780	.297
	2	36.52	2.113	150.520	.409	2.887	86.330	1.541
	3	37.77	3.305	148.490	1.596	6.140	81.055	4.050
	4	39.02	3.262	147.650	.989	6.323	79.890	3.742
4	1	40.27	2.107	148.990	.180	2.235	85.515	.127
	2	41.51	1.202	151.045	1.022	.000	89.967	2.572
	3	42.75	.000	154.382	1.903	.000	90.862	3.529
	4	43.99	.000	154.407	.980	-1.796	96.155	2.140
5	1	45.22	.000	155.620	.656	-2.258	99.520	1.477
	2	46.45	.000	156.052	1.062	-2.609	103.165	1.828
	3	47.67	1.365	152.920	1.863	.000	95.392	3.220
	4	48.89	2.219	149.055	.293	1.426	89.550	.457
6	1	50.10	1.183	151.115	.325	.786	91.095	.461
	2	51.30	2.077	149.385	.947	2.775	87.805	1.841
	3	52.50	2.483	149.135	.841	3.281	88.190	2.725
	4	53.69	1.161	151.615	.654	1.019	91.495	.861

Figure 14.1

RUN 14-1

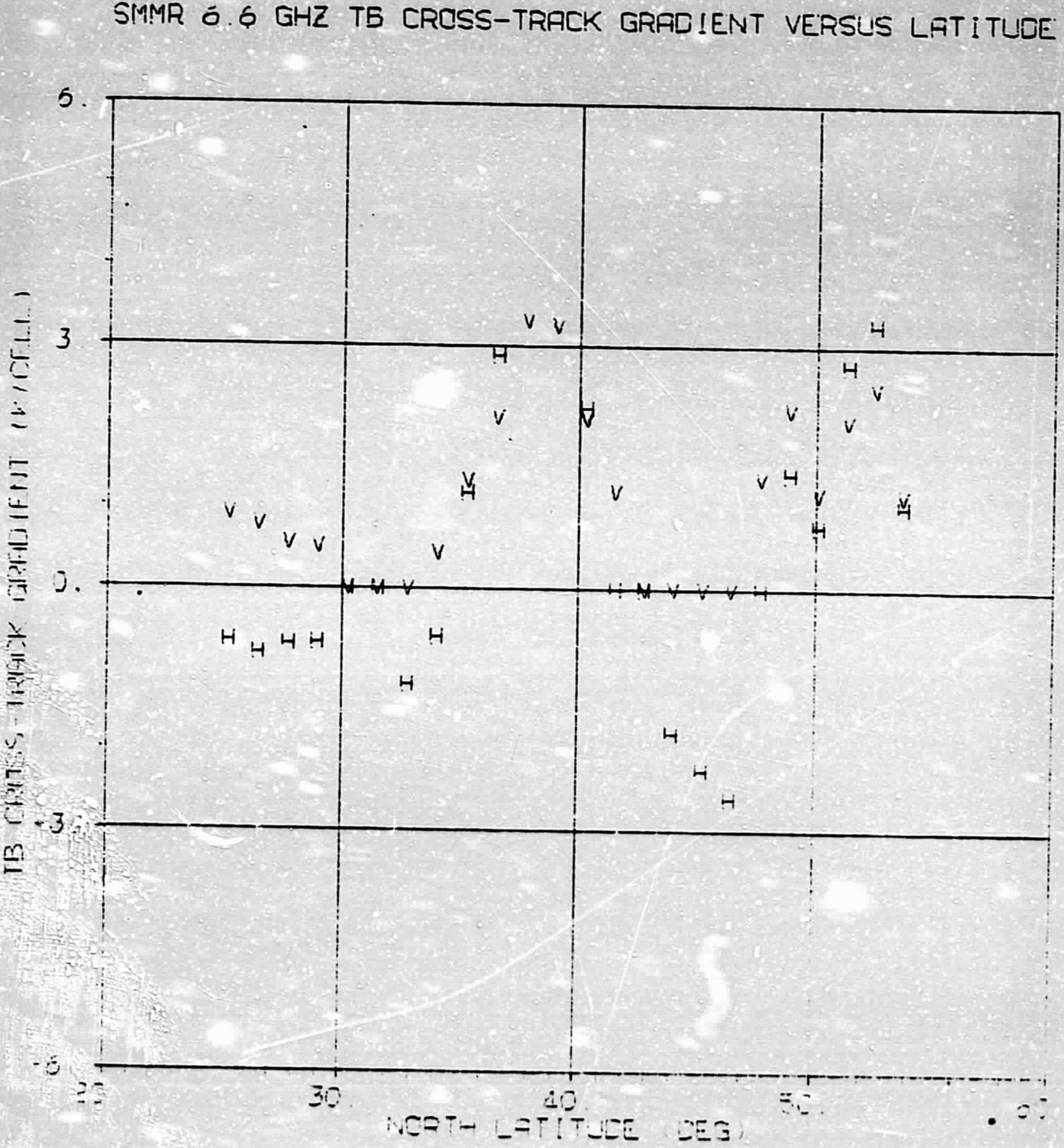

Table 11.2 RUN 11-2

CURVE FITS FOR SMMR 6.6 GHZ VERSUS INCIDENCE ANGLE

	CONSTANT TERM	LINEAR TERM	QUADRATIC TERM	RMS
V POL.	********	-8389.81	85.7169	1.344
H POL.	********	********	197.9298	2.935

Table 12.2 RUN 12-2

CURVE FITS FOR SMMR 6.6 GHZ VERSUS INCIDENCE ANGLE

	CONSTANT TERM	LINEAR TERM	QUADRATIC TERM	RMS
V POL.	********	********	136.1854	.973
H POL.	********	********	441.4208	2.110

Table 13.2 RUN 13-2

CURVE FITS FOR SMMR 6.6 GHZ VERSUS INCIDENCE ANGLE

	CONSTANT TERM	LINEAR TERM	QUADRATIC TERM	RMS
V POL.	82664.45	-3375.74	34.4624	1.370
H POL.	********	-4837.39	49.5412	2.612

Table 14.2 RUN 14-2

CURVE FITS FOR SMMR 6.6 GHZ VERSUS INCIDENCE ANGLE

	CONSTANT TERM	LINEAR TERM	QUADRATIC TERM	RMS
V POL.	23431.55	-947.74	9.5835	2.057
H POL.	844.91	-17.11	-.0000	3.754

Figure 11.2

RUN 11-2

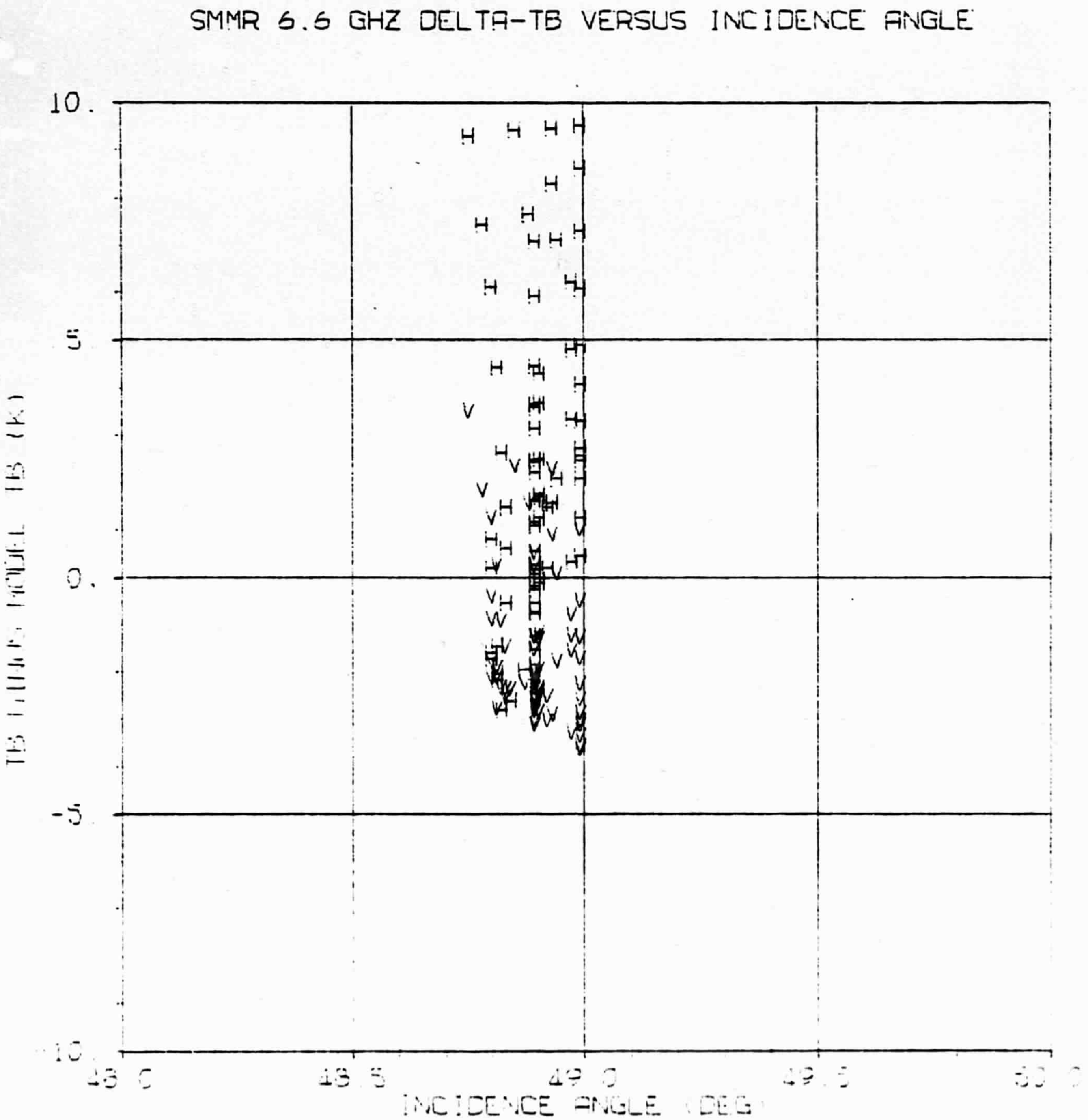

Figure 12.2

RUN 12-2

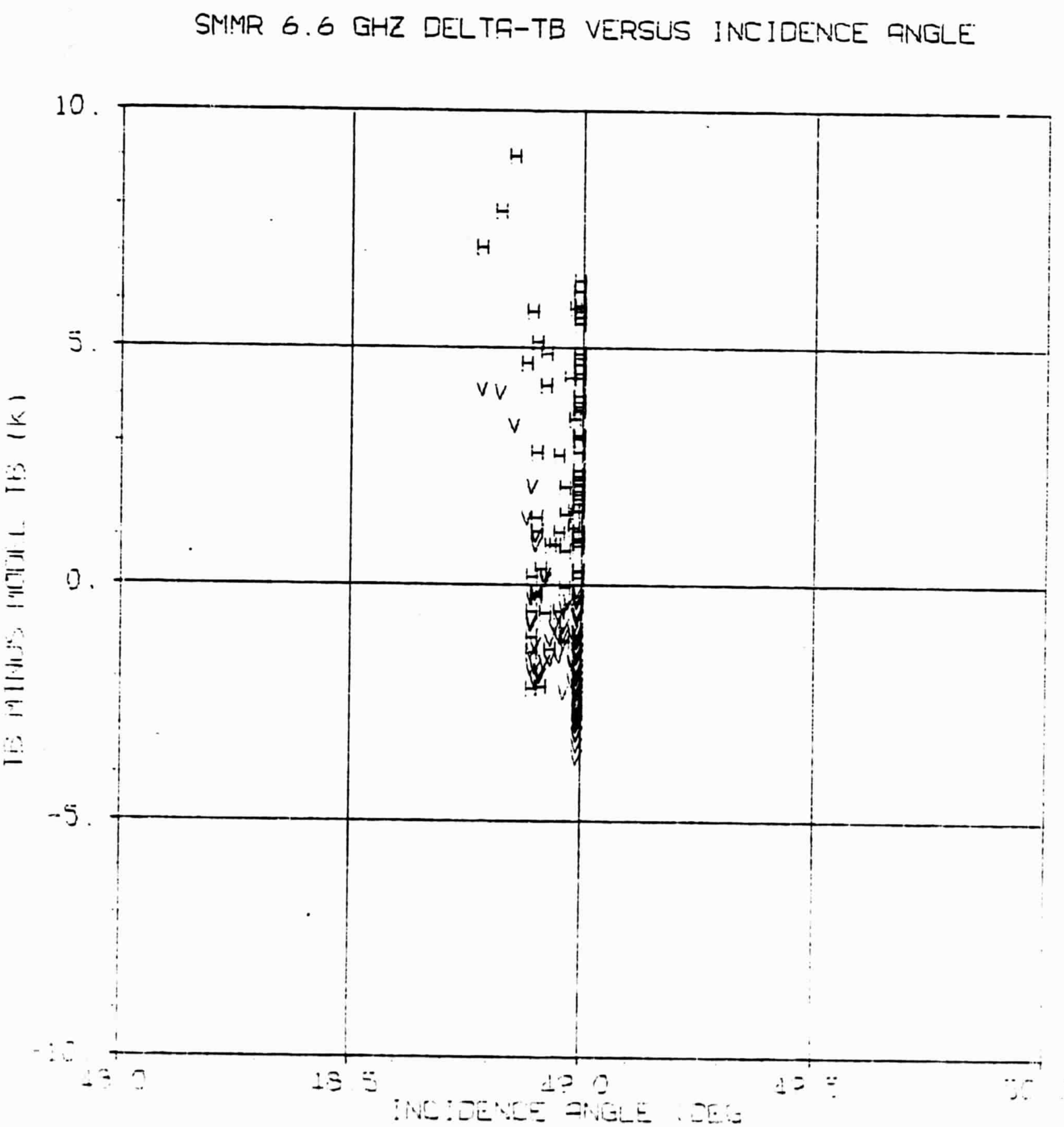

ORIGINAL PAGE IS
OF POOR QUALITY

Figure 13.2

RUN 13-2

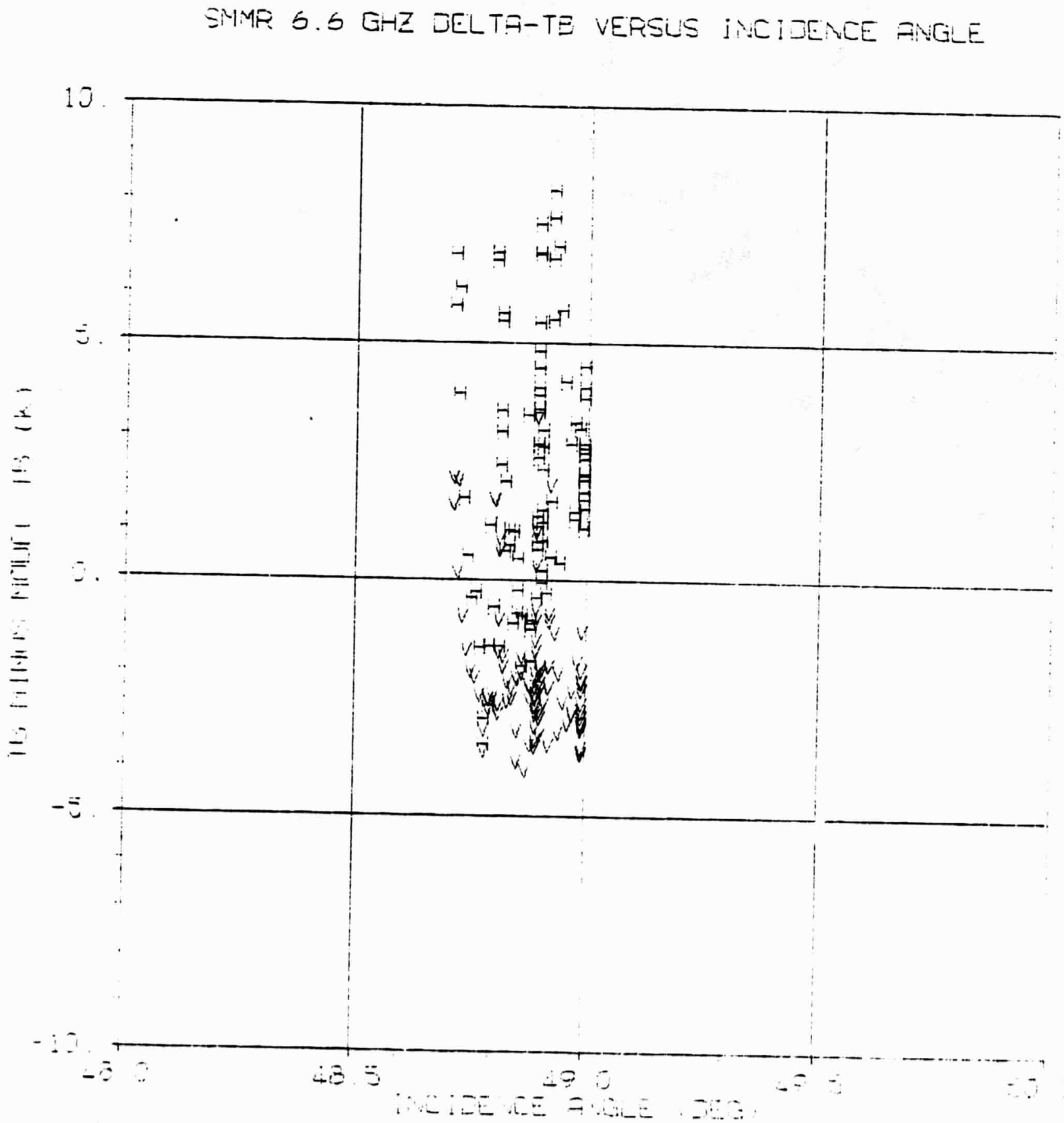

Figure 14.2

RUN 14-2

ORIGINAL PAGE IS
OF POOR QUALITY

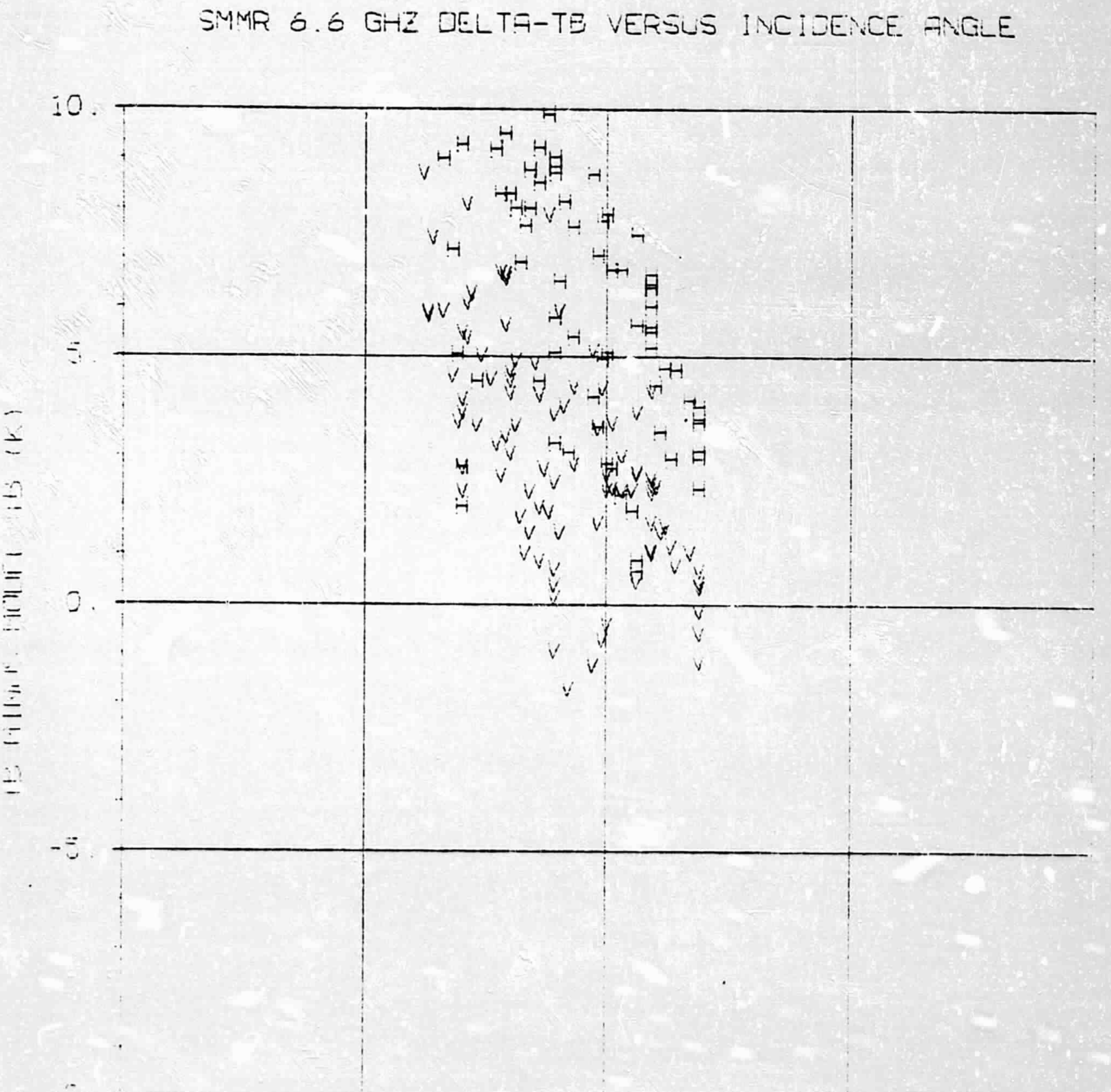

Table 15. Results of 6.6 GHz T_A Data Survey

SEASAT-A Orbit No.	Start Time	No. of Scans	Latitude Span	Min. H Position		Max. V Position	
				Mean	Std. Dev.	Mean	Std. Dev.
1135	257, 9,12,28	19	45^o - 50^oN	9.55	0.83	8.92	0.71
1206	262, 8,31,45	36	24^o - 33^oN	9.46	0.84	8.88	0.50
1207	262,10,12,27	32	25^o - 33^oN	9.31	0.66	8.94	0.52

Times are in Days, Hours, Minutes, Seconds from beginning of year 1978.

Scans refer to SMMR 4.096 seconds scans.